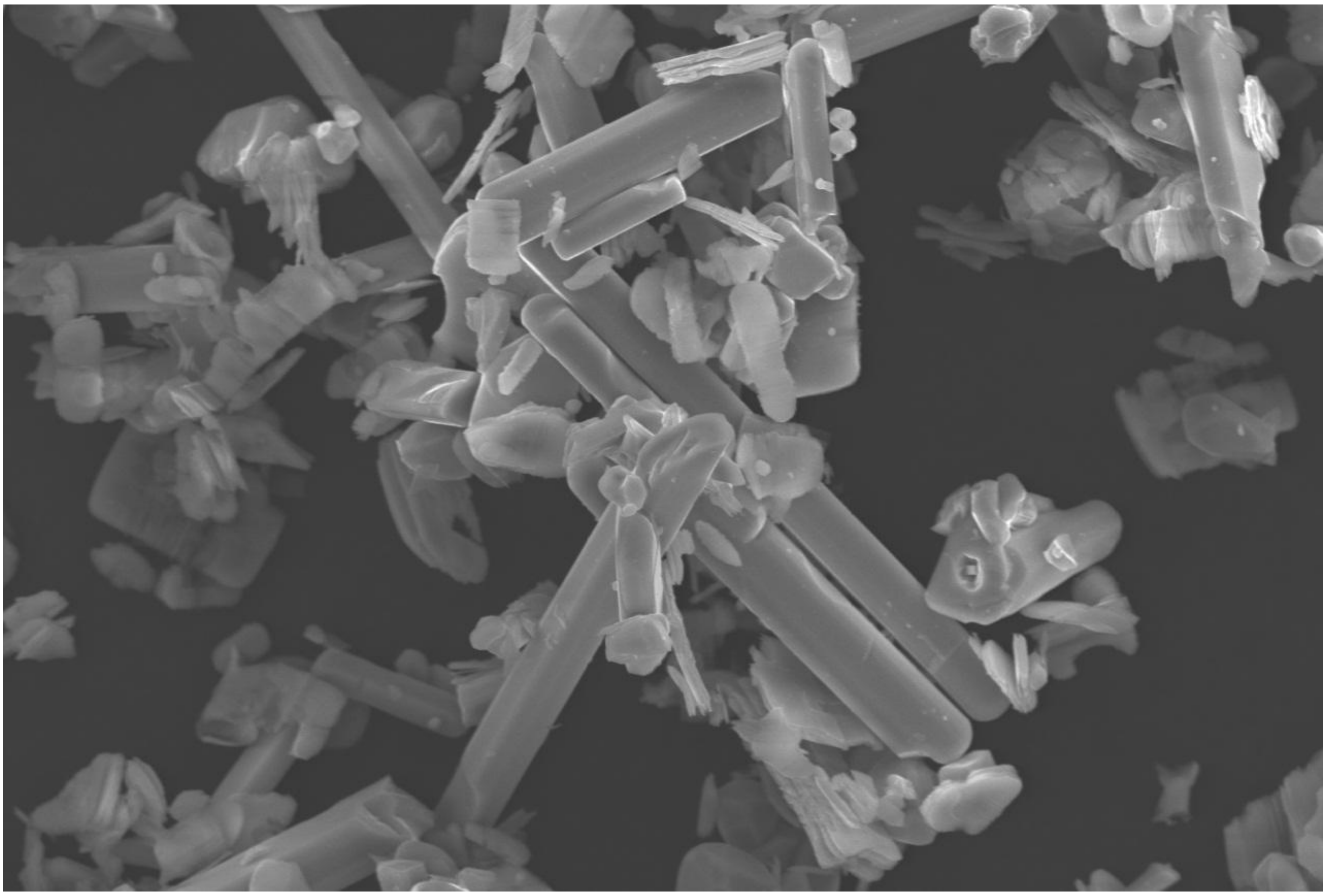

UNIVERSITEIT
TWENTE

RAPID EXFOLIATION OF LAYERED METAL-OXIDES

H. Yuan M.Sc.
Prof.dr.ir. J.E. ten Elshof
Prof.dr.ir. G. Koster
Prof. dr. H.J.M. Bouwmeester

Bachelor Thesis 29-06-2015 | Melvin Timmerman

Abstract

Nanosheets have potential applications in a wide range of fields. Besides the well-known graphene nanosheets, metal-oxide nanosheets are very promising as well. The nanosheets are obtained via exfoliation of their corresponding layered parent-compounds. The exfoliation process is considered to be slow (weeks), but recent studies in the IMS group suggest that the exfoliation process is driven by an acid-base reaction and is a fast process (minutes) for layered metal oxides.

The effect of the reaction time on the morphology and degree of exfoliation is studied of the layered metal-oxide $K_{0.8}Ti_{1.2}Fe_{0.8}O_4$ (KFTO). KFTO is protonated and $H_{0.8}Ti_{1.2}Fe_{0.8}O_4$ (HFTO) is formed. Reaction times with tetrabutylammonium hydroxide (TBAOH, an exfoliating agent) ranging from 30 seconds to 2 weeks are used. The exfoliated nanosheets are deposited on silicon substrates using Langmuir-Blodgett deposition. AFM images are used to determine the morphology and UV-vis spectroscopy is used to determine relations between absorbance and reaction time.

XRD spectra and SEM images confirmed the successful synthesis of KFTO and, its protonated form, HFTO.

The exfoliation of 30 seconds to two weeks reaction times all yielded densely packed nanosheets, with a height of ~1.1nm. Increasing reaction time led to a decrease in nanosheets size from 6.9µm^2 to 3.75µm^2 (reaction time of 30 seconds to two weeks). This is explained by the breaking of the nanosheets due to mechanical shaking.

The trough area at which the deposition took place decreased from 46cm^2 to 31cm^2 and the lift-up point decreased from 77cm^2 46cm^2. This suggests a decrease in concentration of nanosheets, which is explained by restacking of nanosheets into a hybrid state happening at longer reaction times.

The absorbance at 253nm wavelength increased from 0,096 to 0,21. Indicating that there is a higher concentration of nanosheets.

Table of contents

Abstract - 1 -

Introduction - 3 -

- Thesis description - 4 -

Theory - 5 -

- Nanosheets vs. bulk - 5 -
- Metal doped vs. undoped - 5 -
- Exfoliation - 5 -
- Ion intercalation-based exfoliation - 6 -
- Rapid exfoliation - 6 -
- Earlier study on KFTO - 7 -
- Langmuir-Blodgett deposition - 8 -
- Atomic force microscopy - 9 -
- Scanning electron microscopy - 10 -
- X-ray diffraction - 11 -
- UV-vis spectrometer - 11 -

Methods - 13 -

- Preparation of $K_{0.8}[Ti_{1.2}Fe_{0.8}]O_4$ - 13 -
- Protonation - 14 -
- Exfoliation and LB deposition - 14 -
- AFM - 14 -
- UV-vis spectrometer - 14 -

Results and discussion - 15 -

- X-ray diffraction characterization - 15 -
- Scanning electron microscopy analysis - 16 -
- UV-vis spectrometer - 18 -
- Langmuir-Blodgett results - 19 -
- AFM results - 22 -

Conclusions - 26 -

Acknowledgements - 27 -

References - 28 -

Appendix A: UV-Vis measurements - 30 -

Appendix B: Nanosheets size values - 31 -

Appendix C: AFM images - 32 -

Introduction

Delamination of layered compounds is called exfoliation. Exfoliation yields monolayer nanosheets, also known as two dimensional (2D)materials. Graphene nanosheets are well-known, however metal-oxide nanosheets less. Metal-oxide nanosheets are also of great interest. They show advantages as template for growth of oriented functional films, building advanced devices and other applications.[1-3] The nanosheets are normally exfoliated from their layered parent-compounds (i.e. TiO_2 nanosheets from TiO_2 bulk compound).[2, 4]

The potential applications of nanosheets are in the fields of photoinduced, electrochemical, dielectric nanodevices, catalytic and biomedical applications.[3] In thin film growth technology one can tune the properties of thin films via changing its crystallographic orientation.[1] For example, Tebano et al.[5] showed that for films with thicknesses in the range from 3 to 12 nm $La_{0.67}Sr_{0.33}MnO_3$ was insulating on (001) oriented $LaAlO_3$, but behaved as a metal on (110) oriented $LaAlO_3$. Also, the magnetization characteristics and the ferroelectric activity of a material vary by different orientations of the substrate.[1] Functional films could be designed with control over the orientation of a film. This leads to more possibilities for the fabrication of materials. One of the great promises of nanosheets is that different kinds can be deposited on all sorts of amorphous single substrate to locally control the orientation and crystallinity of a film deposited thereon.[1] Nanosheets are also proved to influence the magnetic properties of films. Moreover, the typical dimensions of nanosheets allow to control the orientations of films on much smaller length scales than what is typically achieved on single crystalline substrates, possibly offering unique advantages over costly single crystalline substrates. Another impact nanosheets have, is their dramatic increase in surface area.[6] For surface active or catalytic materials this can greatly enhance their chemical and physical reactivity.

Thesis description

The kinetics of the exfoliation process are considered slow: in literature the exfoliation process normally takes one or more weeks (see Table 1).[1, 4, 7-9] Further development of the exfoliation process is hindered by the slow kinetics. Recent experiments[10] within the Inorganic Materials Science (IMS) research group have shown that the exfoliation process is much more rapid than previously thought (minutes compared to weeks). This study was performed with a well-known study model of layered metal oxides, a layered titanate (potassium lithium titanate, KLTO). The results reveal a different exfoliation mechanism for exfoliation of layered metal oxides compared to previous study. The concept adopted from exfoliation of layered titanates is considered to be a general rule for exfoliation of layered metal oxides. To validate the concept, in this assignment, exfoliation study of another layered titanate, potassium iron titanate (KFTO), is carried out in the IMS group. The main goal of this research is to investigate the influence of the reaction time on the morphology and the degree of exfoliation of the resulting sheets.

Table 1: Different compounds and reaction times for the exfoliation process.

Parent layered oxide	Reference	Exfoliating agent	Duration of reaction
$H_{0.7}Ti_{1.825}O_4$, $H_{1.07}Ti_{1.73}O_4$	[4]	Tetrabutylammonium hydroxide (TBAOH)	8 days
$H_{1.07}Ti_{1.73}O_4$	[1]	TBAOH	21 days
$HCa_2Nb_3O_{10}$	[1]	TBAOH	14 days
$HTiNbO_5$	[7]	TBAOH	7 days
HTi_2NbO_7, HNb_3O_8, $H_4Nb_6O_{17}$	[7]	TBAOH	21 days
$H_{1.07}Ti_{1.73}O_4$	[8]	TBAOH	14 days
K/Mg/Li-stabilized TiO_x	[9]	Tetramethylammonium hydroxide (TMAOH)	7 days
$HCa_2Nb_3O_{10}$, $HTiNbO_5$, HTi_2NbO_7, $H_3Ti_5NbO_{14}$	[11]	TBAOH	10 days

Theory

Firstly the difference between nanosheets and the bulk parent-titanates is described. Secondly, the effect of doping on the compounds is reported. Then the different techniques used are illustrated: the exfoliation process and the Langmuir-Blodgett deposition. Lastly the characterization methods: atomic force microscopy, scanning electron microscopy, X-ray diffraction and UV-vis spectroscopy are outlined.

Nanosheets vs. bulk

The unique 2D structure offers nanosheets distinctive physical and chemical properties in comparison with its bulk compounds.[12] For example $Ti_{0.91}O_2^{0.36-}$ nanosheets show a sharp absorption peak centered at ~265nm, which is dramatically blue-shifted from those of the bulk nanoparticles.[13] Also, the peak-top photon energy for the $Ti_{0.91}O_2^{0.36-}$ nanosheets is approximately 4,67 eV, a lot larger than that of the bulk parent compound.[3] For the electronic properties yields that the band gap energy (Eg) of $Ti_{0.91}O_2^{0.36-}$ is ~3,8 eV. This is around 0.6 eV larger than that of its parent compound.[14] Also, by controlling the nanocrystal growth , TiO_2 with different grown facets such as (001), (010), (101) or (105) have been developed and revealed different surface reactivity in the facet-enriched single crystals. TiO_2 is a material with great facet-control. The understanding of the reactive sites of such anisotropic nanosheets is of significant importance for catalytic applications.[3]

Metal doped vs. undoped

The titania nanosheets have also been reported to be doped with metals, changing the chemical and physical properties. $K_{0.8}Ti_{1.2}Fe_{0.8}O_4$ has an orthorhombic crystal structure.[15] TiO_2 only absorbs UV light and different research activities have been done to develop titanium oxide photocatalysts which can operate effectively on visible light illumination.[16] Fe-substituted as well as Ni-substituted titania nanosheets act as effective photocatalysts.[16, 17] In another study[18] Fe-doped titania nanotubes showed a red shift in the UV-visible absorption spectra and an enhancement of the absorption in the visible region compared to pure titania nanotubes. This would be promising in the field of visible light photocatalysis. The iron doped titania nanosheets also showed decreases in crystallinity and a decrease in the band gap. Fe- and Co-doped titania nanosheets also have promises in short-wavelength magneto-optical applications as well as optical isolators, being more environmental benign compared to other metals used (Cd, Mn and Te) and having less trouble with crystal growth.[19]By doping the crystallinity and the band gap can be decreased, a red shift in the UV-visible absorption spectra can be red-shifted, an enhancement of the absorption in the visible region is realized and mageneto-optical applications could be made of environmentally benign materials.

Exfoliation

Different techniques are used to achieve exfoliation, the delamination of layered compounds. Manual mechanical exfoliation, ultrasonication-assisted solvent exfoliation and ion intercalation-based exfoliation. Manual mechanical exfoliation brings about nanosheets with good properties[20], is very simple[21], but the up scaling is limited by the low yield it provides.[6] Ultrasonication-assisted solvent exfoliation is also simple, but damages the structure of the nanosheets altering the properties and breaking them apart in smaller flakes.[21, 22] Ion intercalation-based exfoliation has a much milder route and yields larger nanosheets, being very promising for future development.[10] This last one will be outlined and used in this research.

Ion intercalation-based exfoliation

Layered materials possess the characteristic to have strong covalent bonds in the layers but weaker layer-to-layer interactions, such as van der Waals or electrostatic attractions.[23] This results in the ability to intercalate ions or solvent between the layers which will induce expansion of the layers, called swelling. Two types of swelling have been documented[23], intracrystalline swelling and osmotic swelling. The first is an increase in the interlayer lattice dimension by the hydration of the gallery species. The latter is the behavior resulting from the penetration of a significant volume of solvent after which the material behaves as a colloidal system.

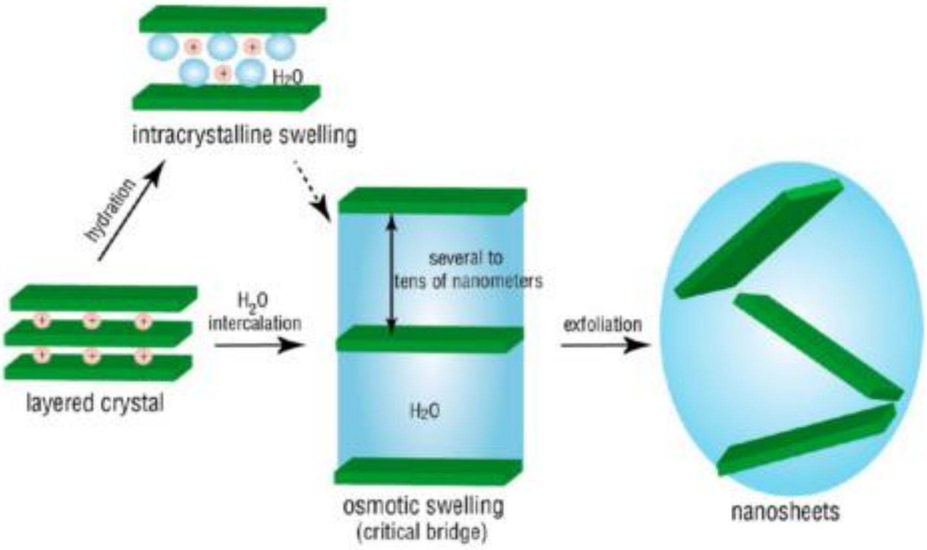

Figure 1: Schematic illustration of swelling and the exfoliation process proposed in literature.[23]

For layered metal oxides with a relatively high layer charge density (like $K_{0.8}[Ti_{1.2}Fe_{0.8}]O_4$), swelling cannot proceed except by replacing the interlayer species with protons followed by reactions in basic solutions.[24] Due to their bronsted solid acidity the protons in the gallery can be further exchanged with organo-ammonium ions in aqueous base solution, for example TBAOH.[2] This is initiated by an acid-base reaction between the protons in-between the layers and the OH^- in the solvent, resulting in water entering the galleries[25], see Figure 1. Ion intercalation is strongly dependent on the available bases in the solution and typically increases with an increasing external base concentration before reaching a saturation value of ~40%. The saturation plateau may be a consequence of reaching an acid-base equilibrium. Infinite swelling leads to the falling apart of the layers into monolayers: exfoliation. This method is very time consuming, see Table 1, which is the main reason it has problems with further development.[6]

Rapid exfoliation

In situ studies[10] have revealed that ion intercalation exfoliation starts directly after adding TBAOH and is a very rapid acid-base reaction. Nanosheets form that can restack into hybrid layered structures. In Figure 2 the different parts of the proposed exfoliation mechanism can be seen. (a): the acid-base reaction starts with diffusion of OH^- into HTO followed by their reaction with protons; (b):

the layered structure of HTO loses its stability because of the acid-base reaction; (c): isolated nanosheets; (d): nanosheets restack into a final hybrid state.

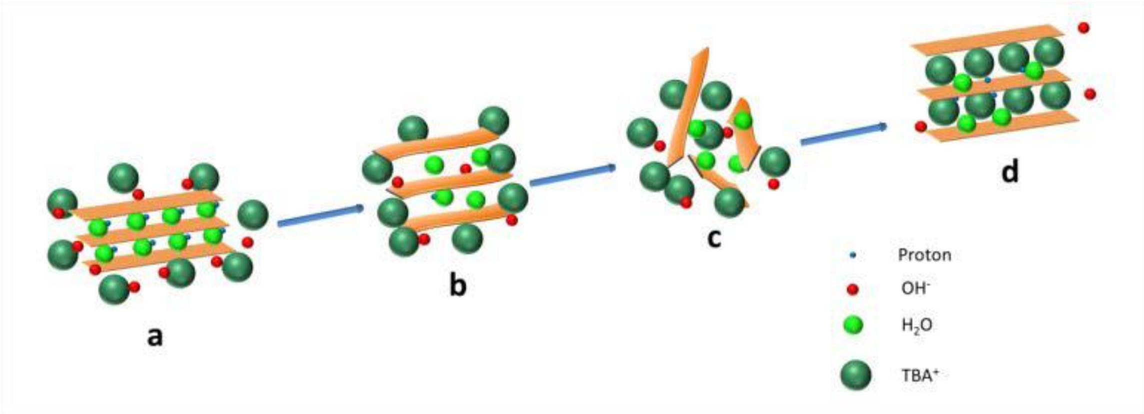

Figure 2: Schematic illustration of the exfoliation and restacking mechanism.[10]

It has been found that the OH^- in the solution reacts quickly with the H^+ in the gallery to form water and to neutralize the interlayer species. This leads to very weak layer-to-layer forces and form, negatively charged, monolayers. These monolayers have to be neutralized by positively charged ions (i.e. TBA^+ and protons).[26]

Earlier study on KFTO

Geng et al.[23] have used the protonated titanium oxide $H_{0.8}[Ti_{1.2}Fe_{0.8}]O_4$ for experiments regarding swelling. They have used different swelling electrolytes namely dimethylethanolamine (DMAE), various tertiary amines (trimethylamine, N,N dimethylethylamine, 3-dimethylamino-1-propanol and N,N-dimethylbutylamine) and quaternary amines (tetramethylammonium hydroxide (TMAOH), diethyldimethylammonium hydroxide (DEDMAOH) and tetrabutylammonium hydroxide (TBAOH)). Different N/H^+ concentration ranges for the added agent was used. At $N/H^+ = 0.5$ a maximum swelling for DMAE and the tertiary amines of 90 nm was reached. For the quaternary ammonium hydroxide solutions the maximum swelling occurred at a lower concentration $N/H^+ = 0.3$ (likely due to the higher osmotic pressure of the starting solutions). For TBAOH the maximum swelling was 98 nm. The stability of the resultant swollen structure is strongly dependent on the chemical nature of the amines or ammonium ions. Species of higher polarity and smaller size, for example DMAE, help stabilize the swollen structure. However, using species of lower polarity and more bulky size, like TBAOH, are prone to trigger exfoliation.[2] Crystals that are swollen in TBAOH have been shown to fall apart easily and exfoliate naturally.[27, 28]

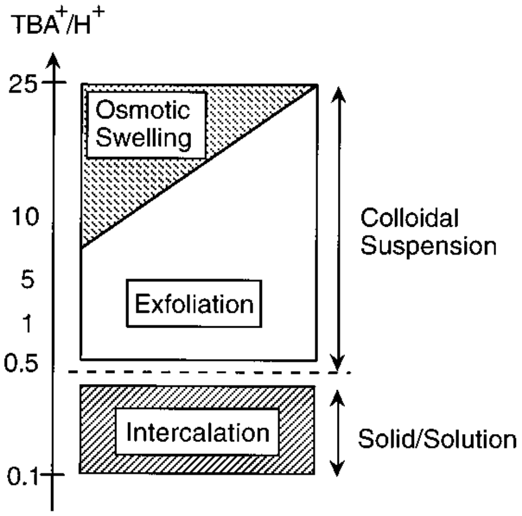

Figure 3: Schematic diagram of the osmotic swelling and exfoliation process, according to literature.[28]

In Figure 3 the ratio between TBA^+ of the exfoliating agent (TBAOH) and H^+ in the layered compounds is illustrated. In this research a ratio of 4:1 is used, to achieve exfoliation.

Langmuir-Blodgett deposition

Langmuir-Blodgett (LB) deposition makes use of the monolayer formation phenomenon of amphiphilic molecules (like TBA^+) to ensure the particles to float at the air-water interface.[3, 29] The interface of monolayered nanoparticles is slowly compressed (by reducing the trough area) and can be deposited by lifting up the solid substrate under a certain surface pressure. When the surface is compressed, the nanosheets will reorganize and form a nearly perfectly packed monolayer, which is a key advantage of LB-deposition. See Figure 4 for a schematic illustration.

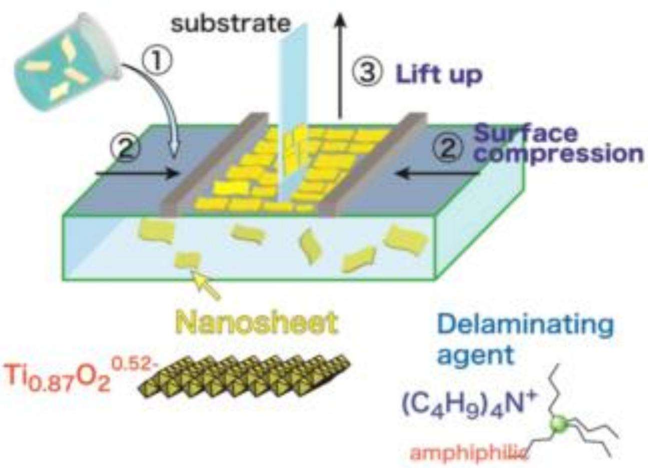

Figure 4: Scheme of LB assembly of $Ti_{0.87}O_2^{0.52-}$ nanosheets.[3]

The transfer to the substrate is a complicated process in which the amphiphiles generally attempt to reach a energetically more favorable configuration as they experience interactions with the solid substrate.[30] LB deposition has a capability to deposit nearly perfectly packed monolayer films under an optimized surface pressure, so it is a powerful technique to study the exfoliation of layered materials.[3] See Figure 5 for an LB-deposition schematic.

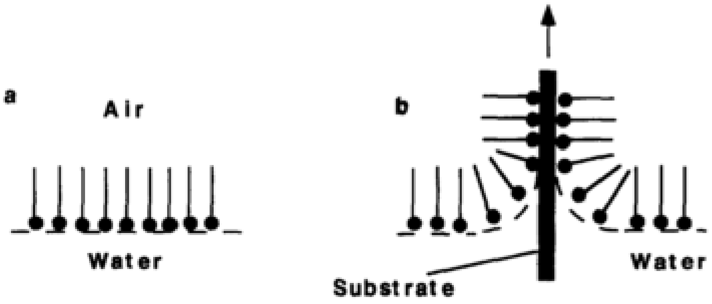

Figure 5: Conventional schematic of the LB deposition process. In (a) the amphiphilic molecules float at the air water interface, in (b) a substrate is vertically lifted upon which the molecules deposit.[30]

A platinum Wilhelmy plate is normally used to measure the surface pressure, which is defined as the difference between the surface tension of the monolayer (γ) and the pure subphase (γ_0), $\Pi = \gamma 0 - \gamma$.[31] The surface tension can be calculated via Wilhelmy's equation: $\gamma = \frac{F}{l \cos(\theta)}$. [32] Here l is the wetted perimeter (2 times the width w and 2 times the thickness d) of the Wilhelmy plate. θ is the contact angle between the surface and the plate.

The transfer rate is calculated via the software. This is the decrease in Langmuir monolayer surface area over the deposited surface area of the substrate.[30] During the deposition of individual nanosheets, the surface area of the monolayers on the water surface (kept at constant surface pressure) decreases due to the transfer of nanosheets to the substrate.

Atomic force microscopy

In an atomic force microscope (AFM) a probing tip is attached to a cantilever.[33] In response to the force between the tip and the sample the cantilever is deflected. Images are taken by scanning the sample relative to the probing tip and digitizing the deflection of the lever. A laser is used and focused on the cantilever. When the cantilever moves due to the interaction with the sample, the (change in the) reflected laser beam is observed. Motions to as small as 0,1 Angstrom can be measured by the deflection sensor. See Figure 6 for a schematic illustration. Here 1 is the laser, 2 is the cantilever, 3 is a mirror, 4 a position sensitive photodetector, 5 electronics and 6 the scanner with a sample.

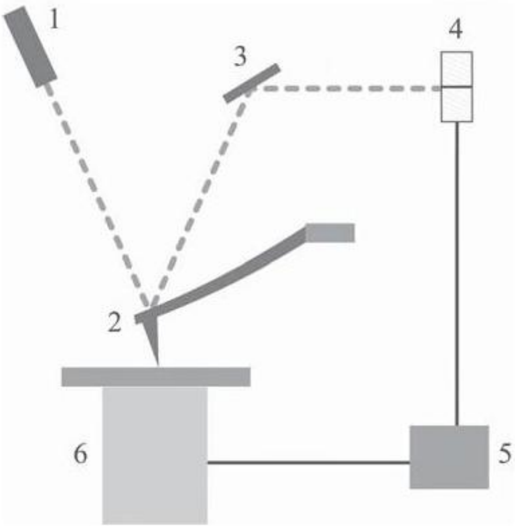

Figure 6: Schematic diagram of an AFM according to [34].

Typical forces between the probing tip and the sample range from 10^{-11} to 10^{-6} N. The interaction force between two covalently bonded atoms is of the order of 10^{-9}N at separations of ~1 Angstrom. This means that non-destructive imaging is possible. There are two force regimes, contact and non-contact mode. When the microscope is operated in non-contact mode at tip-sample separations of 10 to 100 nm, forces, such as van der Waals and electrostatic, can be sensed and give information about surface topography. When the separations are in the order of 1 Angstrom, contact mode can be used, at which the tip touches the surface. In this mode, ionic repulsion forces allow the surface topography to be traced with high resolution. In amplitude modulation atomic force microscopy (AM-AFM, also known as tapping mode) a stiff microlever, which has a sharp tip at its end is excited near its free resonance frequency.[35] The oscillation amplitude is used as a feedback parameter to measure the topography of the sample surface. Material properties variations is mapped by recording the phase shift between the driving force and the tip oscillation. Most experiments in air or in liquids are performed in AM-AFM. The AFM in tapping mode is used in this research to determine the lateral size and the thickness of the nanosheets.[23]

Scanning electron microscopy

In a scanning electron microscope (SEM) a sample is scanned with a focused beam of electrons. The interaction of the electrons with the atoms in the sample is detected and can be translated in the topography and composition of the sample's surface.[36] See Figure 7 for a schematic illustration of a SEM. SEM images are used to determine the morphology of the powders used in this research.

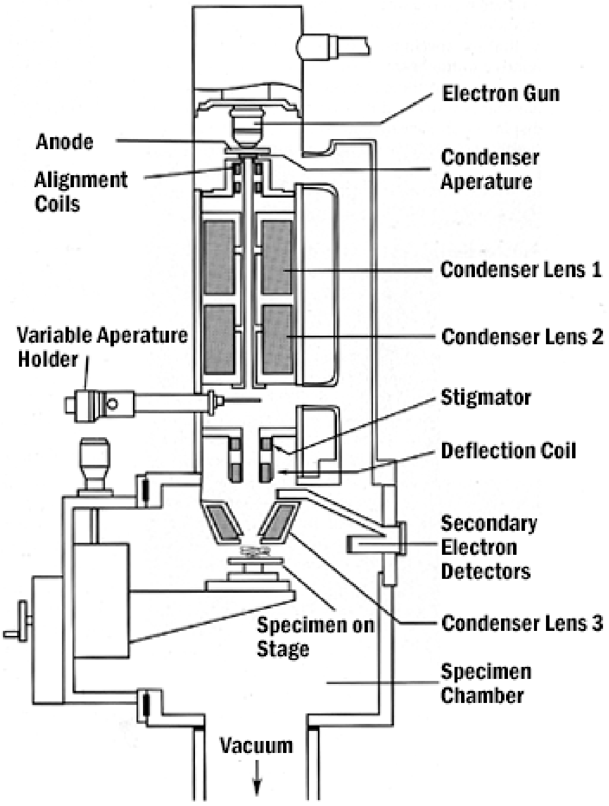

Figure 7: Principles of a SEM.[37]

X-ray diffraction

An X-ray diffraction(XRD)-spectrum can be used to determine the phase purity of the powder. An X-ray diffractometer consists of three basic elements; an X-ray tube, a sample holder and an X-ray detector.[38] The X-rays are generated in a cathode ray tube by heating a filament to produce electrons, accelerating the electrons towards a target by applying a voltage and sending a beam of electrons to the target. When these electrons have sufficient energy to dislodge inner shell electrons of the target material, characteristic X-ray spectra are produced. See Figure 8 for a schematic illustration. For X-ray diffraction Bragg's law is used.[39] It yields: $n\lambda = 2d\sin(\theta)$. Where n is a positive integer, λ the wavelength of the emitted X-rays and θ the diffracted X-rays coming out of the sample. Then d, the (d-)spacing between the atomic layers, can be calculated. For different angles, for example 5 to 60 degrees, and for each diffraction peak, the d-spacing can be used to work out the atomic planes expressed in the Miller indices for that plane (hkl). These phases are characteristic for each compound and have been documented in literature. With XRD can be made sure if the correct crystal is made.

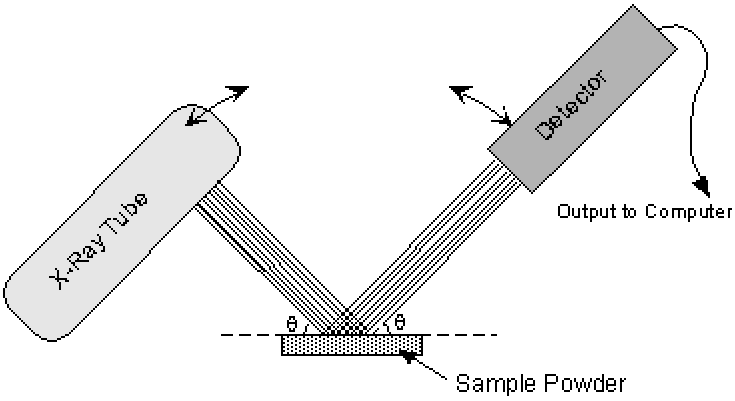

Figure 8: Schematic illustration of an X-ray diffractometer.[39]

UV-vis spectrometer

When an atom or a molecule absorbs energy, electrons can be promoted from their ground state to their excited state. Many inorganic species show charge-transfer absorption and are called charge-transfer complexes. One of the components of an inorganic molecule must have electron donating properties and another component must be able to accept electrons. Absorption of radiation then involves the transfer of an electron form the donor to an orbital associated with the acceptor.[40] In Figure 9 a schematic illustration for a UV-vis spectrometer is shown. Different molecules absorb radiation of different wavelengths. The $Ti_{1.2}Fe_{0.8}O_4$ nanosheets have a peak at a characteristic wavelength, this way is made sure the nanosheets are formed.

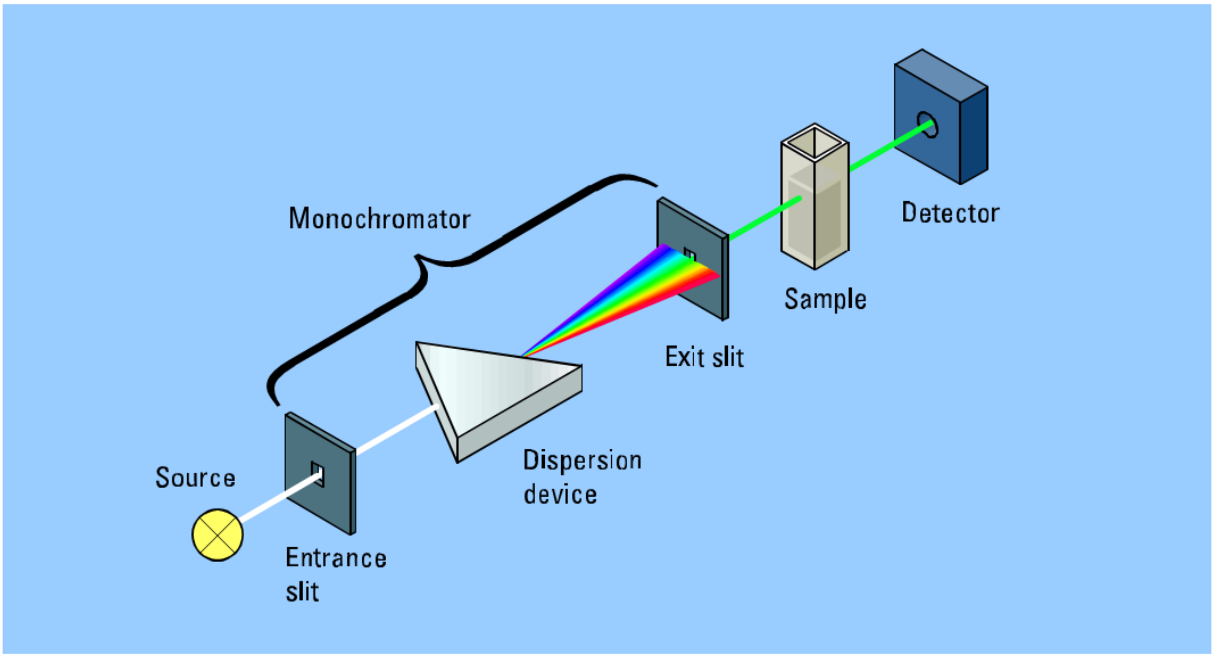

Figure 9: Schematic illustration of an UV-vis spectrometer.[41]

Methods

Preparation of $K_{0.8}[Ti_{1.2}Fe_{0.8}]O_4$

The preparation of the layered parent compound and the protonation thereof was done following Geng et al.[23] A reaction mixture containing the starting materials Titanium(IV) dioxide TiO_2 (Riedel-de Haen), iron oxide Fe_2O_3 (Alfa Aesar), anhydrous potassium carbonate K_2CO_3 (Fluka) and molybdenum (VI) oxide MoO_3 (Sigma-Aldrich) in molar ratio's of: 1.2:0.4:2.03:1.63 were put in a Pt crucible with a tight fitting lid (see Table 2). The mixture was preheated to 900 degrees Centigrade for decarbonation (5 degrees per minute) and kept at 900 for thirty minutes. Then at 5 degrees per minute the temperature was risen to 1150 degrees Centigrade and kept for ten hours. Thereafter at 0.1 degree per minute the temperature was put to 950 degrees Centigrade. The program ended by cooling down to ambient temperature at 5 degrees per minute (see Figure 10). This so-called flux method yields bigger crystals because the diffusivity is higher relative to solid state reactions. [Huiyu Yuan] The crystals were collected from the flux matrix by dissolving the product in water and isolating the crystals by filtration, removing K_2MoO_4. This was done for four days, refreshing the water every day by filtrating and adding fresh water to the residue (where the crystals are). After four days the crystals were air-dried for three days and characterized using a scanning electron microscope (JEOL JSM-6490) and X-ray diffraction (Bruker D2 Phaser).

Table 2: Molar ratio and gram of the different powders used.

	Molar mass (g/mol)	Mol (ratio)	Gram
TiO_2	79.9	1.2	4.792
Fe_2O_3	159.7	0.4	3.194
K_2CO_3	138.2	2.03	14.029
MoO_3	144	1.63	11.73

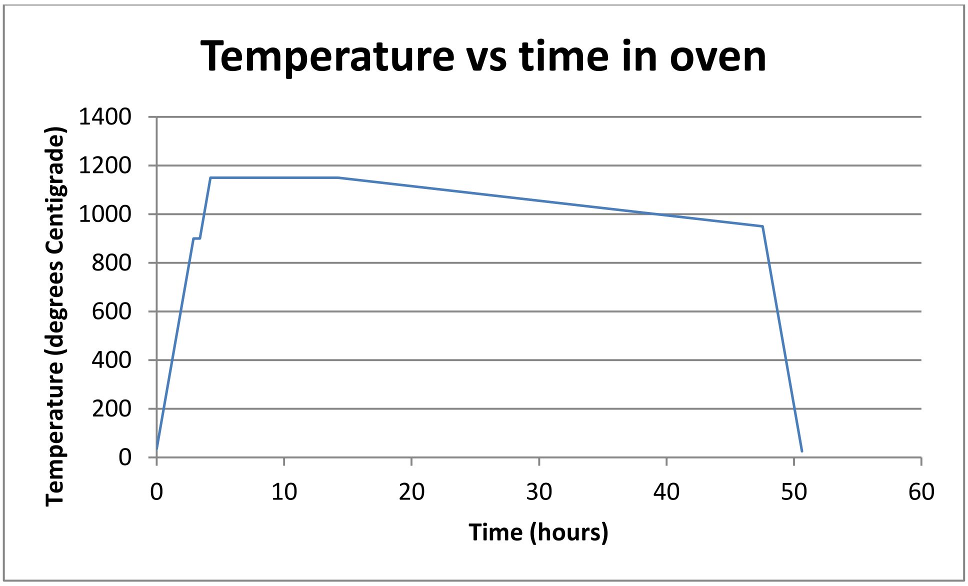

Figure 10: Temperature vs time in oven.

Protonation

$K_{0.8}[Ti_{1.2}Fe_{0.8}]O_4$ is a layered oxide with a relatively high layer charge density. In these types of layered oxides exfoliation cannot proceed except by replacing the interlayer species, potassium, with protons. Followed by reactions in basic solutions, tetrabutylammonium hydroxide (TBAOH), exfoliation can occur. Protonation was achieved by stirring the crystals in 2 mol/dm^3 HCl solution at ambient temperature for 6 days. The acid was replaced twice, after 24h and after 48h of reaction, to ensure complete exchange. Finally, the $H_{0.8}[Ti_{1.2}Fe_{0.8}]O_4.H_2O$ crystals were separated by filtration, washed thoroughly with water, and dried before use.

Exfoliation and LB deposition

0.1 gram of $H_{0.8}[Ti_{1.2}Fe_{0.8}]O_4.H_2O$ crystals was mixed with TBAOH at a molar ratio $OH^- : H^+ = 4 : 1$. After varying reaction times, 5 ml of the stock suspension with nominal concentration 5 g/l was diluted to a volume of 500 ml by addition of water. This diluted solution was kept standing for 5 minutes, then 50 ml was separated using a syringe. After 2 minutes this separated suspension was poured into the LB trough (KSV Minimicro, a Teflon trough with an active surface area of 100 cm^2, length 195 x width 51 x depth 4 mm^3 and a dipping well length 10 x width 28 x depth 28 mm^3, leading to a volume of 48 cm^3) and left for 5 minutes to stabilize the surface pressure before the deposition process started. The film was deposited at the highest surface pressure that was able to reach.
The trough was cleaned prior, and after, every experiment with ethanol and a soft brush, rinsed several times with distilled water to remove ethanol and then blown dry with nitrogen.
The silicon substrates were first cleaned with a CO_2 snow jet to remove dust particles and adsorbates, then it was cleaned in a Harrick Plasma PDC-002 oxygen plasma cleaner (25W) for 15 minutes to oxidize any organic residues on the substrate surface. The substrates were (one in every experiment) immersed vertically into the suspension. The surface pressure was measured using a Wilhelmy plate attached to the KSV minimicro frame. This was also cleaned prior every experiment by rinsing with water, softly blown dry with nitrogen and placed in the plasma cleaner for 15 minutes.

AFM

The Bruker Dimension Icon AFM was used to make images of the nanosheets on the substrates. A silicon cantilever and tip was used. The laser was focused on the cantilever till the reflection was maximum. The position was adjusted so that the laser signal had no deviation. The cantilever was autotuned and automatically approached the surface. The settings like proportional gain, integral gain, amplitude setpoint and scan rate were adjusted until the back and forth signals matched perfectly.
The images were then processed and analyzed using Gwyddion v 2.41, to produce clear images.

UV-vis spectrometer

The solutions for the UV-vis measurements were prepared as for the LB-deposition. Firstly a baseline correction was done with 3mL water. 10 µL of the solution was pipetted to the cuvet and filled till 3mL with water. The measurements were done at a wavelength interval of 500-200nm.

Results and discussion

PXRD patterns and SEM images were made of $K_{0.8}Ti_{1.2}Fe_{0.8}O_4$ and $H_{0.8}Ti_{1.2}Fe_{0.8}O_4$ to characterize the synthesized powder. UV-visible spectra were made of HFTO with TBAOH after the different reaction times. From the LB-setup , several data could be obtained such as the transfer rate, the trough area and the surface pressure. Lastly, the AFM images are discussed.

X-ray diffraction characterization

For both KFTO and HFTO powder-XRD has been used to determine the phase of the powders. An angle of 5 to 60 degrees was used to make sure the interval used in literature (5 to 50 degrees) was covered.

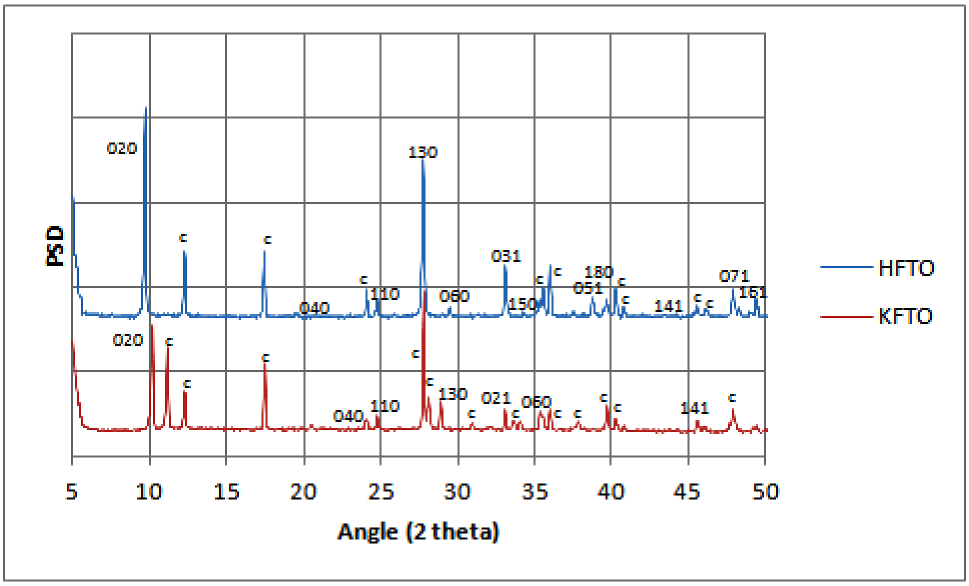

Figure 11: Experimental PXRD spectrum of KFTO (red) and HFTO (blue).

In Figure 11 the peaks for KFTO and HFTO can be seen with the phases according to literature.[16, 23] However, there is some contamination at high intensities. The peaks that are indicated with a "c" is the contamination (for KFTO at an angle of ~11, 12, 17, 27, 37, 40 and 48 and for HFTO at an angle of ~12, 17, 24, 36, 40 and 46). These peaks could not be identified by literature research and use of different software applications. This leads to uncertainty about KFTO and HFTO being the only layered material in the powder. At the AFM section the nanosheets on the substrate are investigated. Peaks that are corresponding with KFTO show a little shift to a lower angle when they are in the HFTO spectrum. This is because the potassium is switched with H_3O^+ which increases the space between the layers.

Scanning electron microscopy analysis

For both dried powders of KFTO and HFTO SEM images were made to determine the morphology.

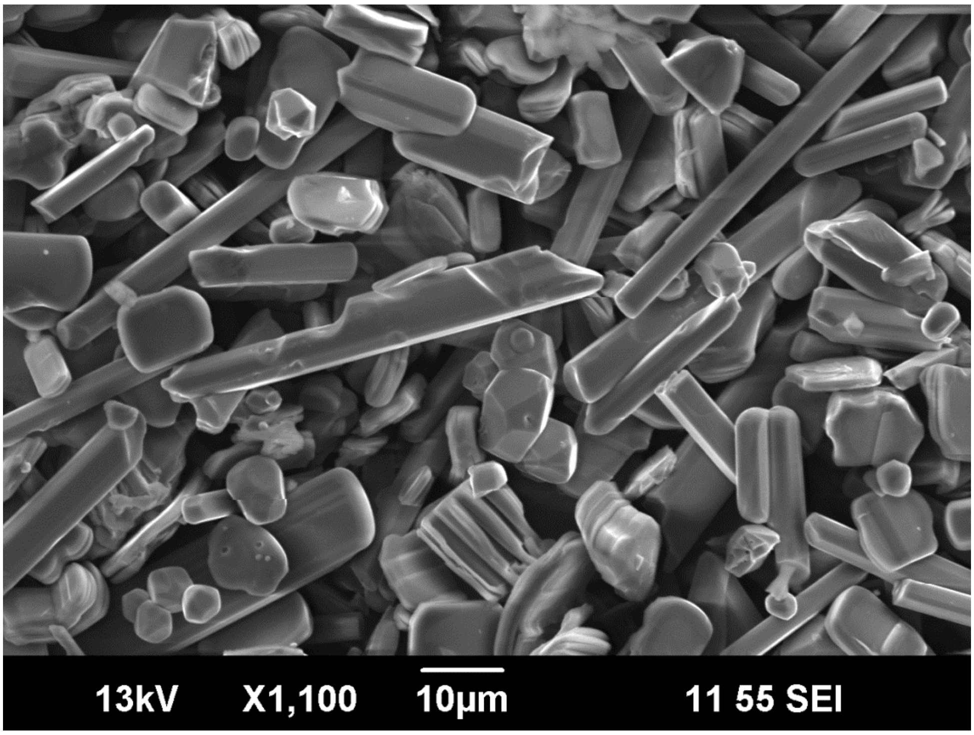

Figure 12: SEM image of $K_{0.8}Ti_{1.2}Fe_{0.8}O_4$ (KFTO).

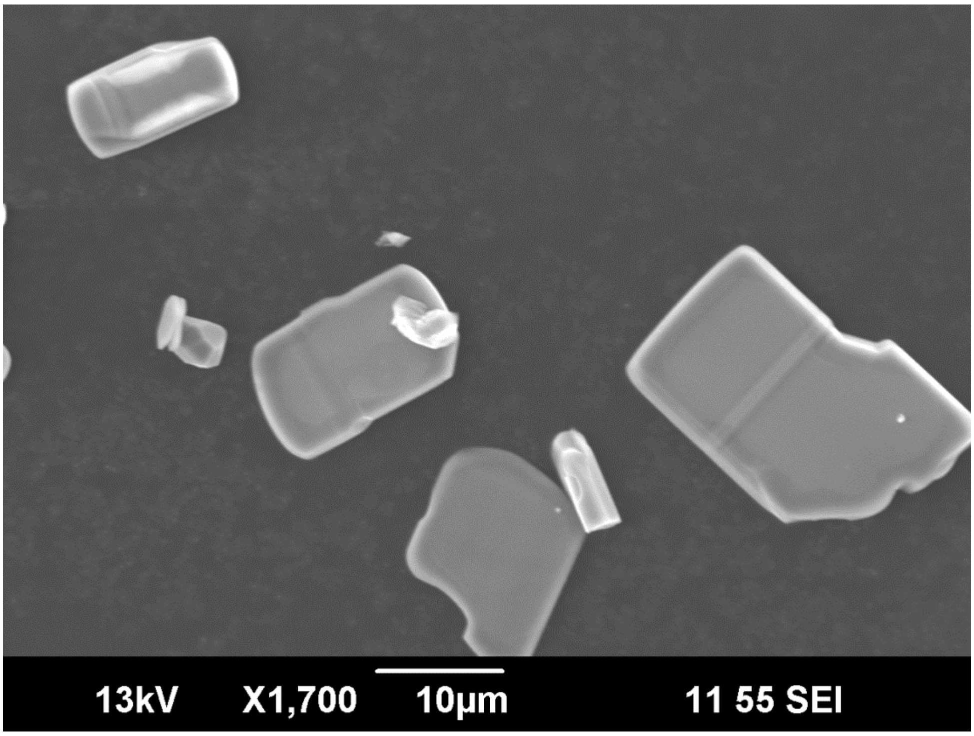

Figure 13: SEM image of KFTO.

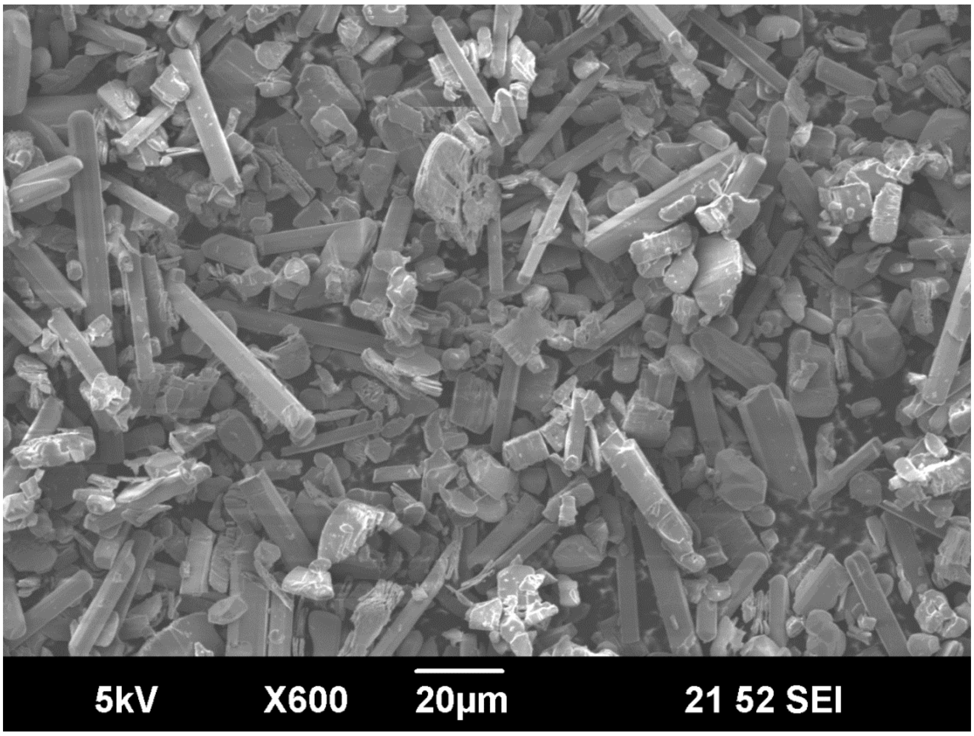

Figure 14: SEM image of $H_{0.8}Ti_{1.2}Fe_{0.8}O_4$ (HFTO).

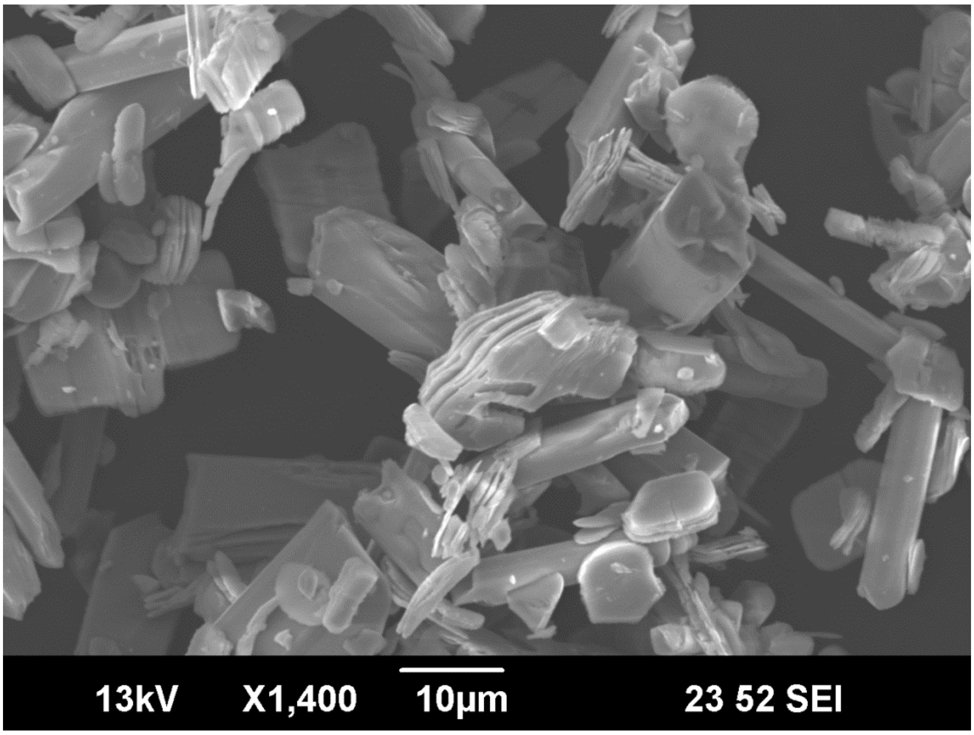

Figure 15: SEM image of HFTO.

The width (8-10µm), the length (10-15µm) and the flatness of the powder, shown in Figure 13, correspond to the SEM image for KFTO in literature[23] and is probably the layered titanate. The layeredness of the material can be seen, especially in Figure 15. The longer (30+µm) rectangular "rods" are probably the contamination, these do not correspond to SEM images in literature. The ratio of contamination to KFTO or HFTO seems to be large, corresponding to the high intensity in the

PXRD patterns for the contamination. The HFTO SEM images do not differ much from the KFTO SEM images. This is likely due to the only difference being the change from potassium to hydrogen.

UV-vis spectrometer

For reaction times ranging from 30 seconds to nine days, UV-vis spectroscopy measurements were made triplicate. There seems to be a peak at 253 nm, this is according to literature.[16]

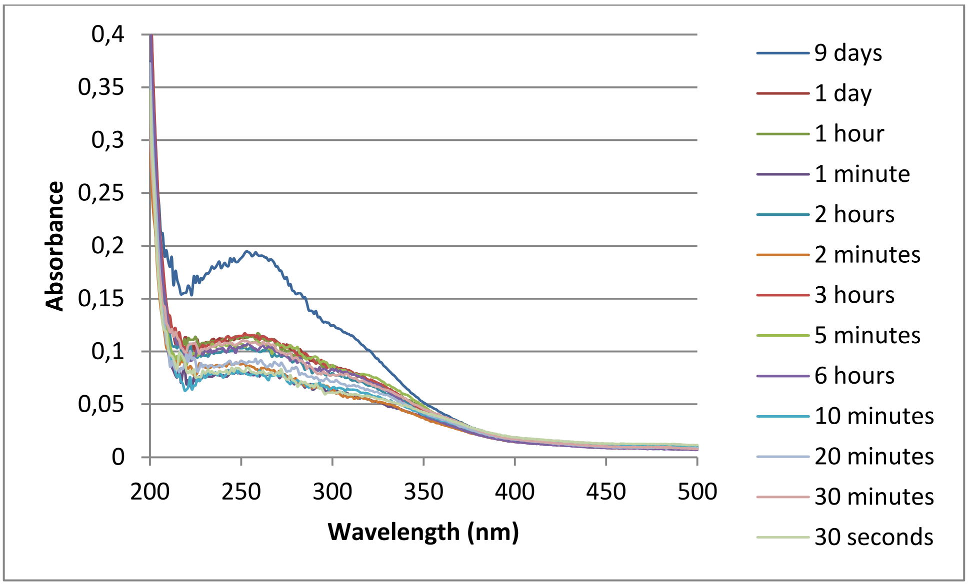

Figure 16: UV-vis spectrum of the first measurement.

The triplicated measurements were averaged at 253 nm wavelength, the mean deviation was calculated as the errorbars and plotted versus the reaction time (see Figure 17).

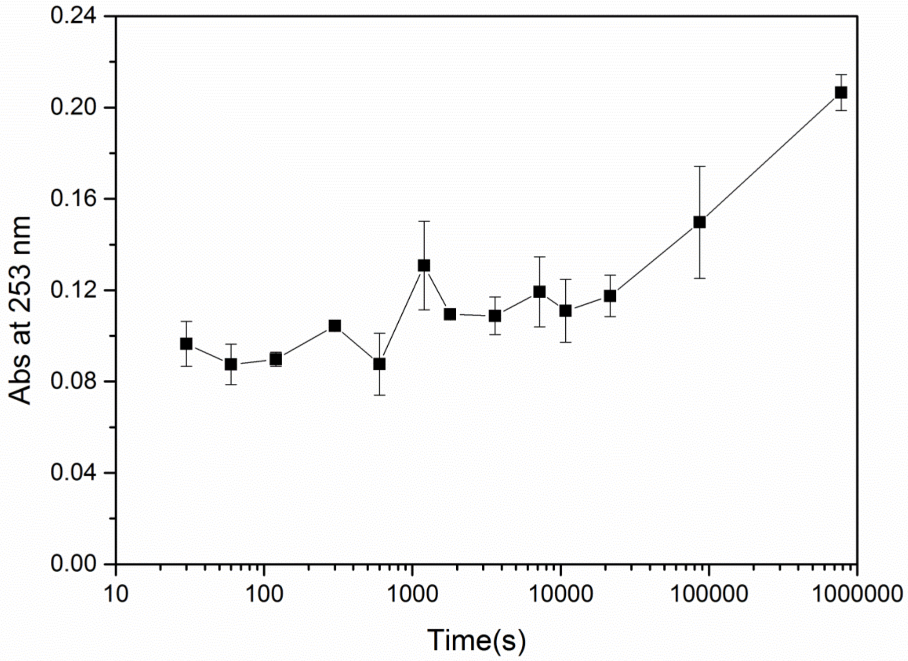

Figure 17: Mean absorbance at 253 nm versus the reaction time.

The absorbance is highest with a reaction time of 9 days. After that comes the one day reaction time. The lowest absorbance is seen at the shortest reaction times. It seems like the absorbance increases with increasing reaction time, suggesting more entities that exhibit absorbance. This indicates that there is a higher concentration of nanosheets. However, the XRD-data showed that there was contamination, which could also be the reason for the increase. In the chapter of the AFM results, the nanosheets are investigated.

Langmuir-Blodgett results

For the different reaction times, values are measured such as: the exact grams HFTO used, the surface pressure that was reached after the first five minutes of stabilizing, the (maximum) surface pressure at which the deposition took place, the transfer rate, the trough area that was used during the deposition, and the lift-up point. The surface pressure and the trough areas were measured as follows.

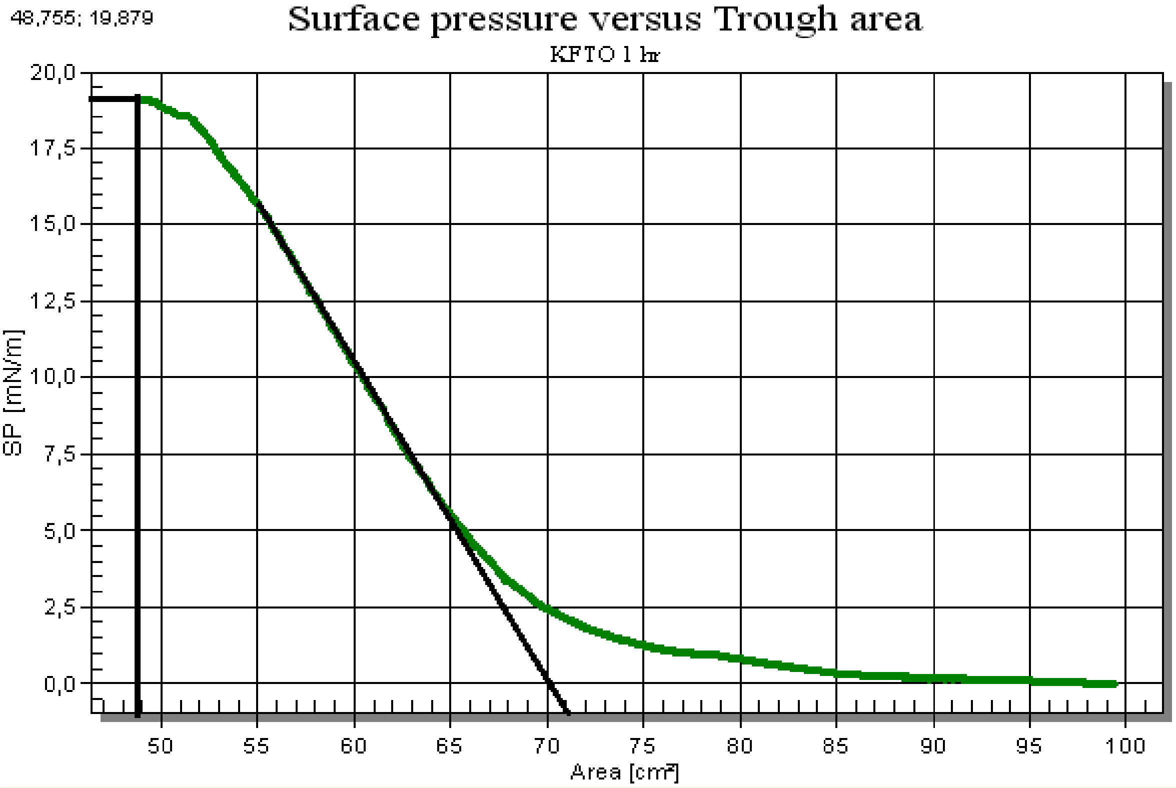

Figure 18: Determination maximum surface pressure, trough area slope and deposition trough area.

In Figure 18 the green line is what the software shows. The black line following the slope of the green line till it intersects the x-axis is how the lift-up point is measured (71 cm^2 in this case). The horizontal and vertical lines from the end of the green line (this is when the deposition starts), show the deposition surface pressure, here can clearly be seen that this is the maximum surface pressure, and the deposition trough area respectively (19 mN/m and 48,8 cm^2 respectively in this case). In Table 3 the LB-results are shown for the different reaction times.

Table 3: Langmuir-Blodgett deposition results. Exact grams HFTO used: 0.1±0.0008.

Reaction time	Maximum surface pressure after closing barrier (mN/m)	Transfer rate	Deposition trough area (cm^2)	Lift up point (cm^2)
15 seconds	**19.5**	**4.447**	**46**	**77**
30 seconds	**20.1**	**6.384**	**46.9**	**87**
30 seconds	Setup broke	Setup broke	Setup broke	Setup broke
30 seconds	*14.5*	*0.886*	*/////////////*	*/////////////*
1 minute	**17.6**	**3.544**	**57.2**	**82**
1 minute	*11.1*	*-0.559*	*/////////////*	*/////////////*
2 minutes	**18.6**	**4.021**	**55**	**83**
5 minutes	**20.6**	**3.473**	**39.8**	**60**
5 minutes	*18.7*	*3.512*	*/////////////*	*/////////////*
10 minutes	**18.2**	**2.248**	**50.3**	**73**
20 minutes	**19.1**	**6.17**	**55.6**	**88**
30 minutes	**20.3**	**3.853**	**41.7**	**67**
1 hour	**19**	**3.122**	**48.8**	**71**
1 hour	16.9	3.348	60.4	95
2 hours	**19.4**	**3.265**	**43.3**	**63**
2 hours	*18.7*	*3.472*	*/////////////*	*/////////////*
3 hours	**17.2**	**2.585**	**50.9**	**78**
3 hours	*16.1*	*-0.488*	*/////////////*	*/////////////*
6 hours	**20.1**	**3.849**	**39**	**59**
1 day	20.2	9.65	39.5	87
1 day	**21.4**	**4.369**	**34.4**	**54**
1 week	**16.5**	**5.287**	**34.1**	**56**
2 weeks	**19.5**	**3.477**	**31**	**46**

The italic reaction times 30 seconds, 1 minute, 5 minutes, 2 hours and 3 hours were experiments where the LB-setup was not calibrated correctly yet (these were the first five measurements). This led to incorrect trough areas that could not be used for further analysis. However, in principle the substrates did undergo deposition, so these were analyzed with the AFM. The 30 seconds reaction time that is not in bold nor italic was an experiment where the barrier touched another part of the setup which resulted in the barriers to stop working. The substrates from the reaction times 1 hour and 1 day that are not in bold nor italic were checked with the AFM and resulted in no nanosheets or very little dispersed over the substrates. These reaction times were done over.
The data in bold were ultimately used for analysis. In Figure 19 and Figure 20 the lift up point, the trough area during deposition and the surface pressure during deposition can be seen versus the reaction times (logarithmic scale in seconds).

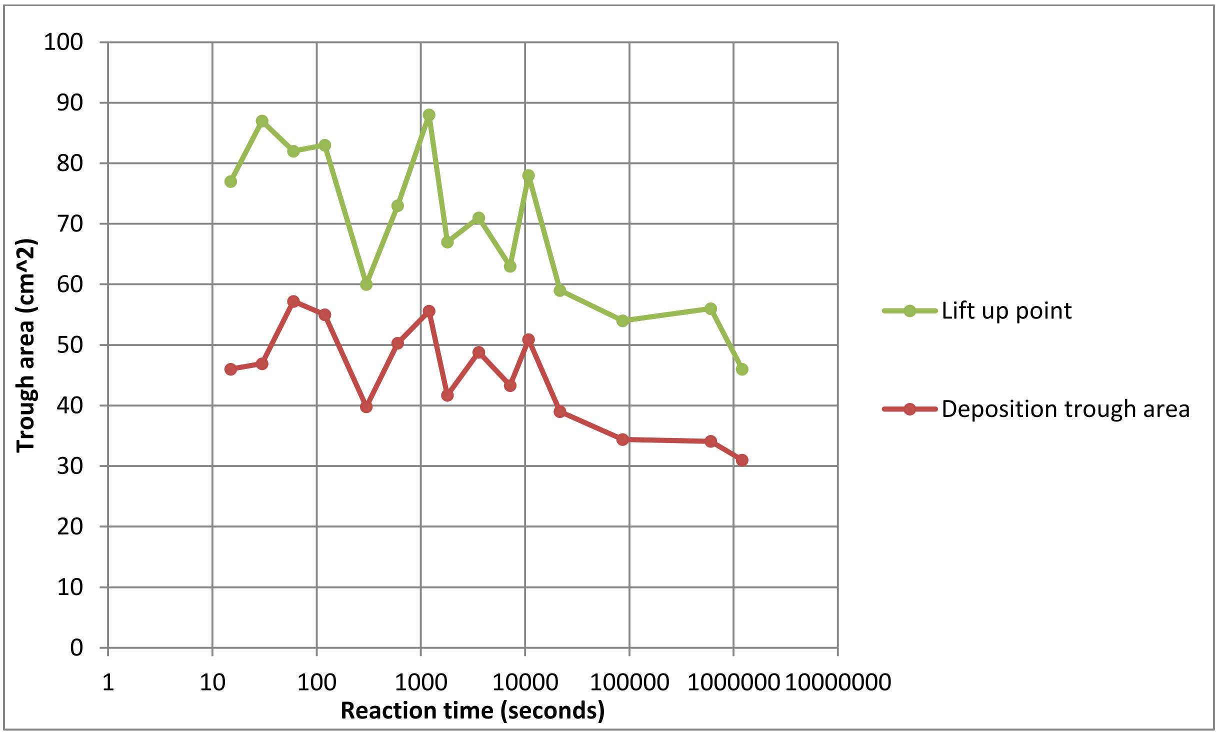

Figure 19: Lift up point and deposition trough area versus reaction time.

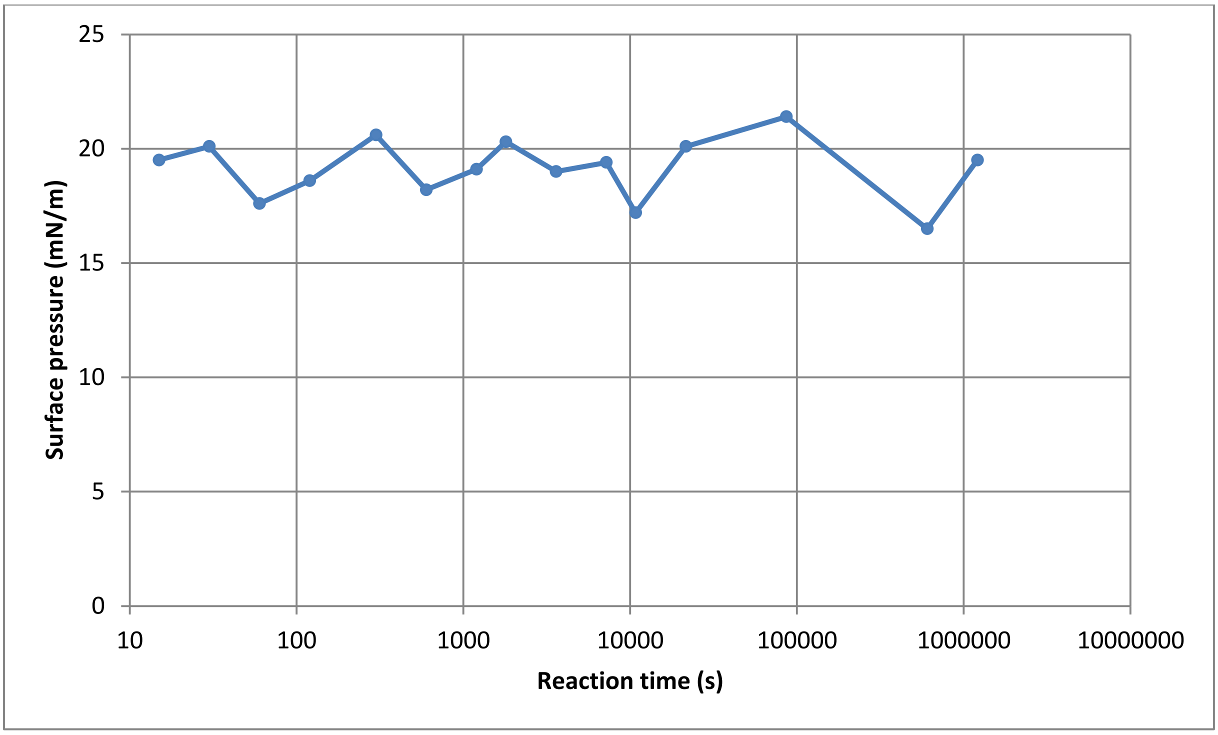

Figure 20: Surface pressure versus reaction time.

It seems like the trough areas, both used for deposition and from the lift-up point, show a decrease with increasing reaction time. This suggests a decrease in surface area of the nanosheets, indicating less concentration of nanosheets. There seems to be a connection between the lift-up point and the deposition trough area. For example, they both go down at 300 seconds and both have a peak at 1200 seconds. The trough area and the lift-up point are both in connection with the concentration of the nanosheets. When the nanosheets concentration is lower, the trough area should also be smaller to achieve the same resultant nicely packed monolayer. The lift-up point should therefore also be lower, because otherwise the deposition does not go well. An explanation for this could be when the reaction time increases, more nanosheets are being restacked, resulting in a lower concentration of monolayer nanosheets, resulting in a smaller trough area.

The influence of the reaction time on the surface pressure is negligible. This could be explained, because the same nanosheets should somewhat have the same surface pressure when they get closer to a nicely packed monolayer.

AFM results

The bold reaction times in Table 3 showed good nanosheets (a densely packed film) except for the 15 seconds one. In Figure 21 and Figure 22 the nanosheets for the 30 seconds reaction time and the height of the nanosheets can be seen respectively. The height difference can be seen on the right of the image. The nanosheets are visible (higher, lighter) on the substrate (lower, darker).

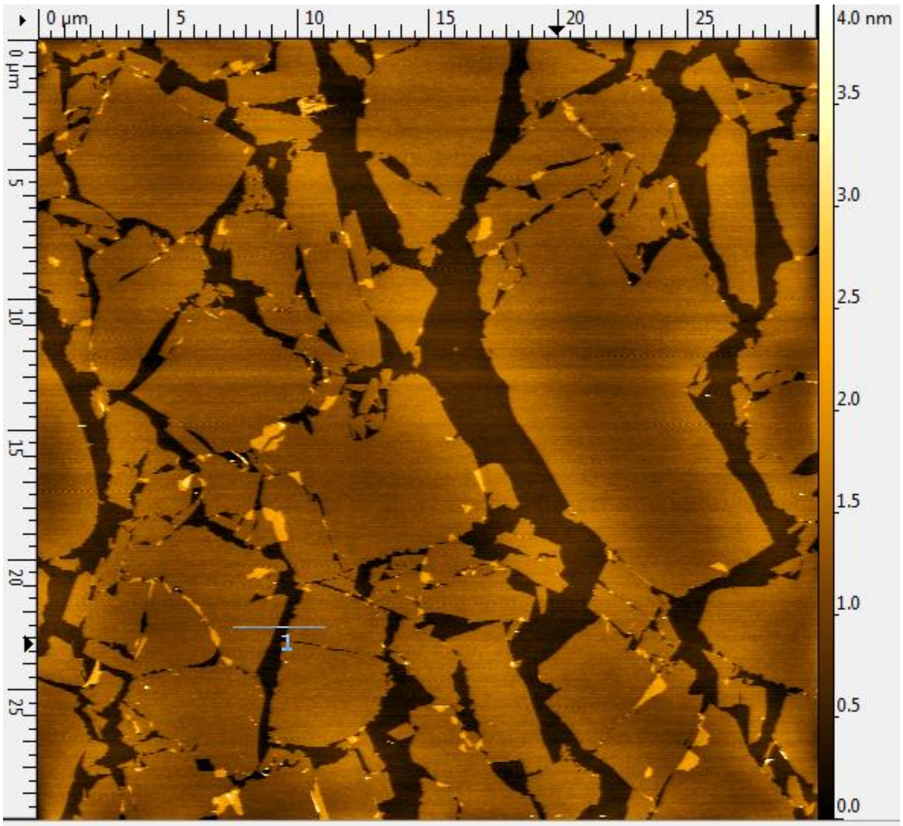

Figure 21: AFM image of 30 seconds reaction time.

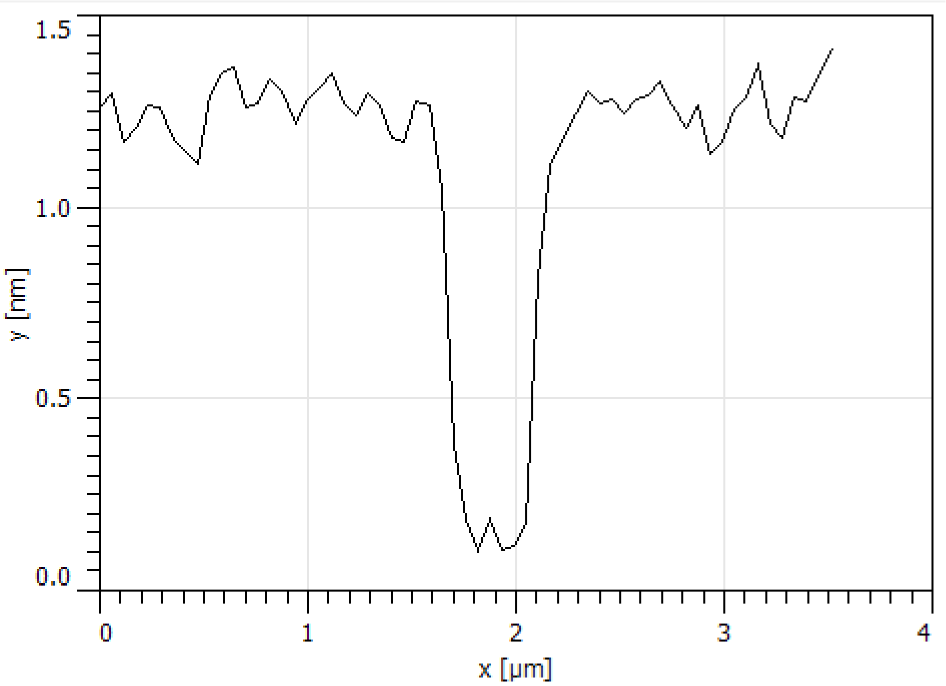

Figure 22: Height difference of line 1 in Figure 21.

In Figure 21 can be seen that after only 30 seconds reaction time, nanosheets have already been formed. The height of the nanosheets are ~1.1nm on all substrates (see Figure 22, ~0.2nm is the substrate and ~1.3nm is a monolayer of nanosheets), corresponding to literature for $Ti_{1.2}Fe_{0.8}O_4$.[23]

For all samples, the mean nanosheets size has been measured and plotted versus the reaction time. This is done by evaluating the amount of nanosheets divided by the total area (see Figure 25). For comparison, Figure 23 shows the sheets from the 1 hour reaction time and Figure 24 shows those from the 2 weeks reaction time.

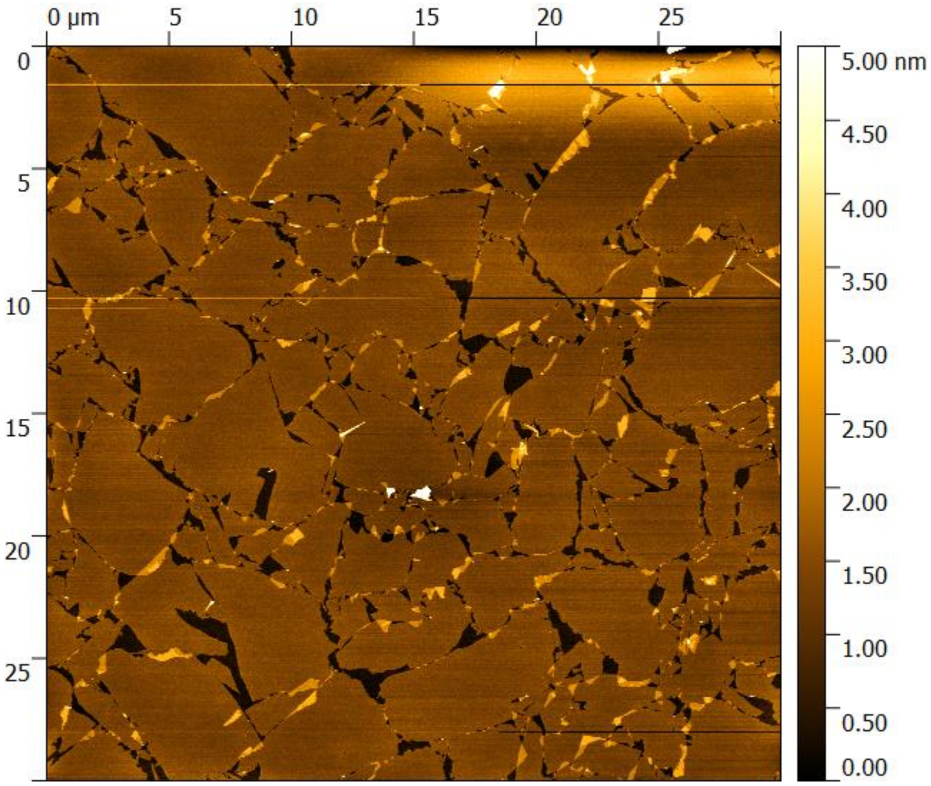

Figure 23: AFM image of nanosheets formed after 1 hour of reaction time.

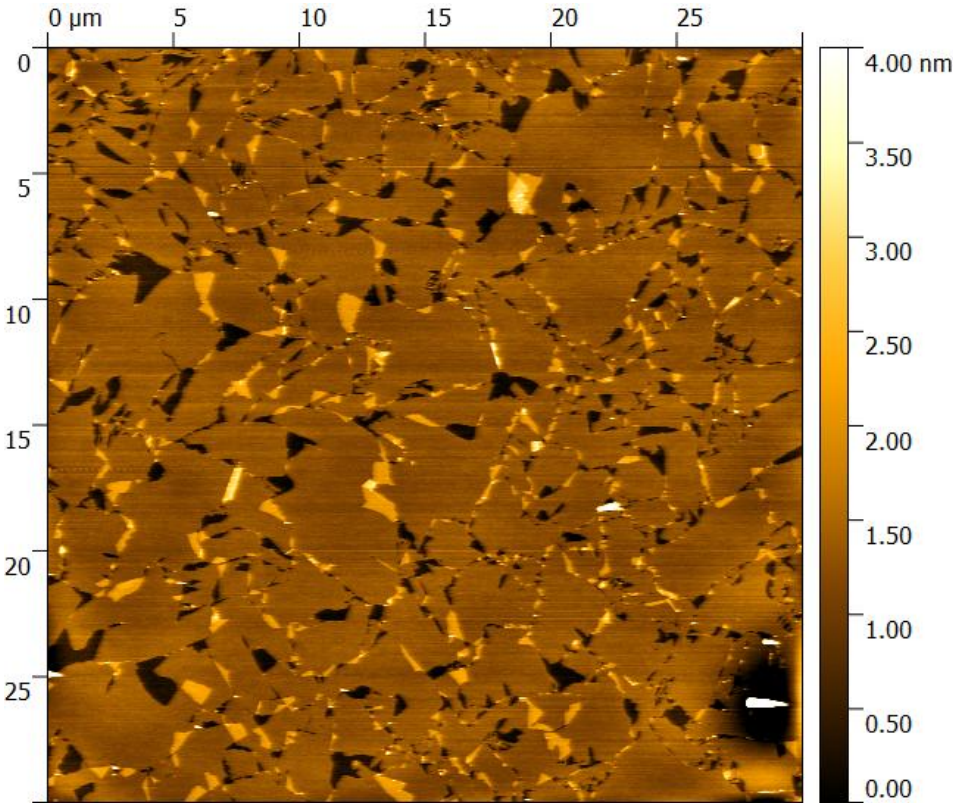

Figure 24: AFM image of nanosheets formed after 2 weeks of reaction time.

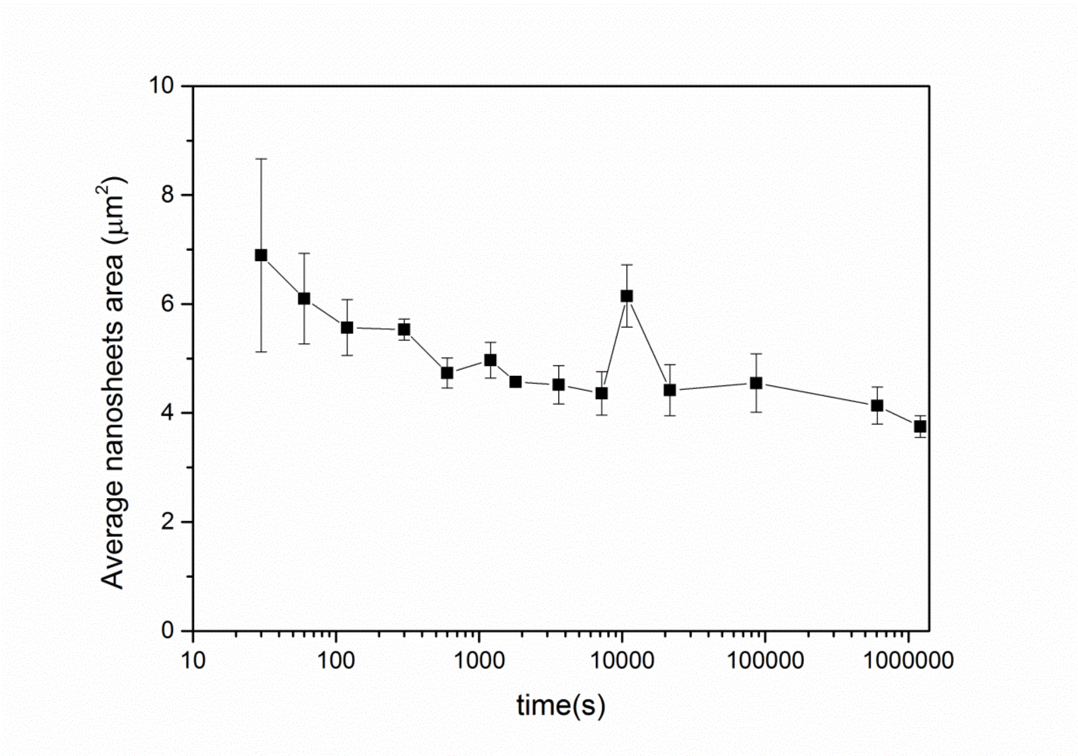

Figure 25: Mean size of the nanosheets versus reaction time (logarithmic scale).

The Figures 21, 23 and 24 suggest a decrease in surface area of the nanosheets. Figure 25 also suggests a decrease in surface area with increasing reaction time. This could be because of the longer (mechanical) stirring breaking the nanosheets, which has been documented in literature to be possible.[42]

Conclusions

From the XRD and SEM characterizations it can be concluded that KFTO and HFTO is both succesfully synthesized, however there is a considerable amount of contamination. The XRD data could not be analyzed as to what this contamination might be, which leaves the effect of the contamination unknown. The size of the KFTO and HFTO crystals formed are 8-10µm by 10-15µm, corresponding to literature.

The scope of this research was to investigate the influence of the reaction time on the obtained nanosheets. First of all, nanosheets have been formed after only 30 seconds of reaction time. This is much faster than the weeks reaction time used in literature (see Table 1). The data obtained from the LB-deposition showed a decrease in lift-up point and deposition trough area when the reaction time is increased. This suggests a decrease in concentration of nanosheets, which could be explained due to the probable restacking of the nanosheets to a final hybrid state (see Figure 2). The reaction time did not influence the surface pressure used for the deposition.

The AFM images show a densely packed monolayer of nanosheets on reaction times varying from 30 seconds to two weeks. The height is ~1.1nm, according to literature. The average size of the nanosheets seem to decrease with increasing reaction time. This could be explained by the breaking of the nanosheets in smaller ones by the mechanical shaking used. This has also been documented in literature.

The absorbance in the UV-visible spectrum seem to increase with increasing reaction time. Indicating a higher concentration of nanosheets. More entities of the nanosheets could exhibit absorbance, leading to a higher absorbance. This is contradictory to the LB-data results. More research should be done to confirm the UV-data.

Acknowledgements

I would like to thank Huiyu Yuan for guiding me through this first experience with research, his tips and tricks, his time and patience. I would also like to thank André ten Elshof for giving me insight in my report and presentation. I would like to thank research group Inorganic Materials Science (IMS) for giving me the time and space to finish my Bachelor's degree. Dominic Post for giving me a training on the SEM, Karin van den Nieuwenhuijzen for giving me the lab instruction and Werner Wessels for giving me the AFM training. From the PCS group I would like to thank Kai Han for giving me the XRD training. I would also like to thank Thimo te Molder for reading through my report and giving comments where needed.

References

1. Nijland, M., et al., *Local control over nucleation of epitaxial thin films by seed layers of inorganic nanosheets.* ACS applied materials & interfaces, 2014. **6**(4): p. 2777-2785.
2. Ma, R. and T. Sasaki, *Two-Dimensional Oxide and Hydroxide Nanosheets: Controllable High-Quality Exfoliation, Molecular Assembly, and Exploration of Functionality.* Accounts of chemical research, 2014.
3. Wang, L. and T. Sasaki, *Titanium Oxide Nanosheets: Graphene Analogues with Versatile Functionalities.* Chemical Reviews, 2014. **114**(19): p. 9455-9486.
4. Yuan, H., et al., *Improved Langmuir–Blodgett Titanate Films via in Situ Exfoliation Study and Optimization of Deposition Parameters.* ACS applied materials & interfaces, 2014. **6**(11): p. 8567-8574.
5. Tebano, A., et al., *Interplay between crystallographic orientation and electric transport properties in La 2/3 Sr 1/3 MnO 3 films.* Applied physics letters, 2010. **96**(9): p. 092505-092505-3.
6. Nicolosi, V., et al., *Liquid Exfoliation of Layered Materials.* Science, 2013. **340**(6139).
7. Dias, A.S., et al., *Exfoliated titanate, niobate and titanoniobate nanosheets as solid acid catalysts for the liquid-phase dehydration of d-xylose into furfural.* Journal of Catalysis, 2006. **244**(2): p. 230-237.
8. Nakato, T., Y. Yamashita, and K. Kuroda, *Mesophase of colloidally dispersed nanosheets prepared by exfoliation of layered titanate and niobate.* Thin Solid Films, 2006. **495**(1–2): p. 24-28.
9. Lee, S., et al., *Exfoliation of titanium oxide powder into nanosheets using hydrothermal reaction and its reassembly into flexible papers for thin-film capacitors.* Journal of Solid State Chemistry, 2015. **224**(0): p. 76-81.
10. Huiyu Yuan, D.D., Rogier Besselink and Johan E. ten Elshof, *The Rapid Exfoliation and Subsequent Restacking of Layered Titanates Driven by Acid-Base reaction.* 2015.
11. Akatsuka, K., et al., *Electronic band structure of exfoliated titanium-and/or niobium-based oxide nanosheets probed by electrochemical and photoelectrochemical measurements.* The Journal of Physical Chemistry C, 2012. **116**(23): p. 12426-12433.
12. Coleman, J.N., et al., *Two-Dimensional Nanosheets Produced by Liquid Exfoliation of Layered Materials.* Science, 2011. **331**(6017): p. 568-571.
13. Sasaki, T. and M. Watanabe, *Semiconductor nanosheet crystallites of quasi-TiO2 and their optical properties.* The Journal of Physical Chemistry B, 1997. **101**(49): p. 10159-10161.
14. Sakai, N., et al., *Electronic band structure of titania semiconductor nanosheets revealed by electrochemical and photoelectrochemical studies.* Journal of the American Chemical Society, 2004. **126**(18): p. 5851-5858.
15. Groult, D., C. Mercey, and B. Raveau, *Nouveaux oxydes à structure en feuillets: Les titanates de potassium non-stoechiométriques K x (MyTi 2− y) O 4.* Journal of Solid State Chemistry, 1980. **32**(3): p. 289-296.
16. Harada, M., et al., *Preparation and characterizations of Fe- or Ni-substituted titania nanosheets as photocatalysts.* Journal of Photochemistry and Photobiology A: Chemistry, 2002. **148**(1–3): p. 273-276.
17. Zhou, M., J. Yu, and B. Cheng, *Effects of Fe-doping on the photocatalytic activity of mesoporous TiO 2 powders prepared by an ultrasonic method.* Journal of Hazardous Materials, 2006. **137**(3): p. 1838-1847.
18. Teng, H., et al., *Preparation of Fe-doped nanotubes and their photocatalytic activities under visible light.* International Journal of Photoenergy, 2013. **2013**.
19. Osada, M., et al., *Gigantic magneto-optical effects induced by (Fe/Co)-cosubstitution in titania nanosheets.* Applied Physics Letters, 2008. **92**(25): p. 253110-253110.
20. Soldano, C., A. Mahmood, and E. Dujardin, *Production, properties and potential of graphene.* Carbon, 2010. **48**(8): p. 2127-2150.

21. Ambrosi, A., et al., *Electrochemistry of Graphene and Related Materials.* Chemical Reviews, 2014. **114**(14): p. 7150-7188.
22. Mas-Balleste, R., et al., *2D materials: to graphene and beyond.* Nanoscale, 2011. **3**(1): p. 20-30.
23. Geng, F., et al., *Gigantic swelling of inorganic layered materials: A bridge to molecularly thin two-dimensional nanosheets.* Journal of the American Chemical Society, 2014. **136**(14): p. 5491-5500.
24. Auerbach, S.M., K.A. Carrado, and P.K. Dutta, *Handbook of layered materials*. 2004: CRC Press.
25. Geng, F., et al., *Unusually stable ~100-fold reversible and instantaneous swelling of inorganic layered materials.* Nat Commun, 2013. **4**: p. 1632.
26. Elshof, J.E.t., *Hearing.* 2015.
27. Ma, R. and T. Sasaki, *Nanosheets of oxides and hydroxides: Ultimate 2D charge-bearing functional crystallites.* Advanced Materials, 2010. **22**(45): p. 5082-5104.
28. Sasaki, T. and M. Watanabe, *Osmotic swelling to exfoliation. Exceptionally high degrees of hydration of a layered titanate.* Journal of the American Chemical Society, 1998. **120**(19): p. 4682-4689.
29. Yang, P. and F. Kim, *Langmuir–Blodgett Assembly of One-Dimensional Nanostructures.* ChemPhysChem, 2002. **3**(6): p. 503-506.
30. Schwartz, D.K., *Langmuir-Blodgett film structure.* Surface Science Reports, 1997. **27**(7–8): p. 245-334.
31. Talham, D.R., *Conducting and magnetic Langmuir-Blodgett films.* Chemical reviews, 2004. **104**(11): p. 5479-5502.
32. Butt, H.-J., K. Graf, and M. Kappl, *Physics and chemistry of interfaces*. 2006: John Wiley & Sons.
33. Meyer, E., *Atomic force microscopy.* Progress in Surface Science, 1992. **41**(1): p. 3-49.
34. Braga, P.C. and D. Ricci, *Atomic force microscopy: biomedical methods and applications*. Vol. 242. 2004: Springer Science & Business Media.
35. García, R. and R. Pérez, *Dynamic atomic force microscopy methods.* Surface Science Reports, 2002. **47**(6–8): p. 197-301.
36. McMullan, D., *Scanning electron microscopy 1928–1965.* Scanning, 1995. **17**(3): p. 175-185.
37. *Scanning Electron Microscopy*. Available from: http://cmrf.research.uiowa.edu/scanning-electron-microscopy.
38. Dutrow, B.L. and C.M. Clark. *X-ray Powder Diffraction (XRD)*. Available from: http://serc.carleton.edu/research_education/geochemsheets/techniques/XRD.html.
39. Nelson, S.A. *X-ray Crystallography*. 2014; Available from: http://www.tulane.edu/~sanelson/eens211/x-ray.htm.
40. SheffieldHalamUniversity. *UV-Vis Absorption Spectroscopy*. Available from: http://teaching.shu.ac.uk/hwb/chemistry/tutorials/molspec/uvvisab1.htm.
41. Garces, F.O. *UV Vis Absorption Spectroscopy*. Available from: http://faculty.sdmiramar.edu/fgarces/LabMatters/Instruments/UV_Vis/Cary50.htm.
42. Maluangnont, T., et al., *Osmotic swelling of layered compounds as a route to producing high-quality two-dimensional materials. A comparative study of tetramethylammonium versus tetrabutylammonium cation in a lepidocrocite-type titanate.* Chemistry of Materials, 2013. **25**(15): p. 3137-3146.

Appendix A: UV-Vis measurements

Reaction time (seconds)	Absorbance	(mean)Deviation
30	0.096479	0.009888
60	0.087465	0.008885
120	0.08967	0.00308
300	0.104453	0.001133
600	0.087565	0.013624
1200	0.13085	0.019394
1800	0.109453	0.001425
3600	0.10879	0.008202
7200	0.119296	0.015316
10800	0.111003	0.013815
21600	0.117538	0.009098
86400	0.14973	0.024535
777600	0.206542	0.00782

Appendix B: Nanosheets size values

Reaction time (seconds)	Mean surface area (μm^2)	(mean)Deviation (μm^2)
30	6,895445	1,771222
60	6,100009	0,829306
120	5,56895	0,512131
300	5,532305	0,194374
600	4,734638	0,275258
1200	4,971742	0,326629
1800	4,569834	0,069834
3600	4,518882	0,352661
7200	4,360517	0,402184
10800	6,14736	0,570555
21600	4,419837	0,468653
86400	4,551619	0,536691
604800	4,135797	0,341154
1209600	3,753169	0,199065

Appendix C: AFM images

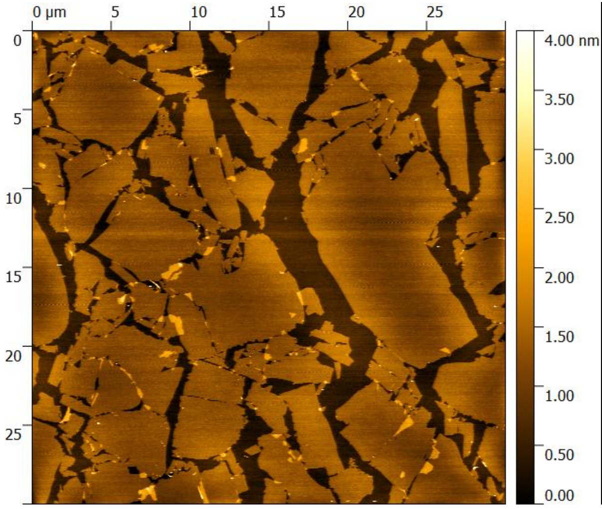

30 seconds

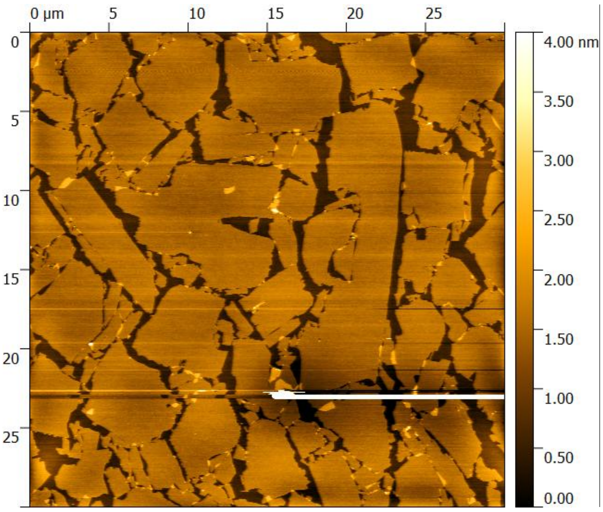

1 minute

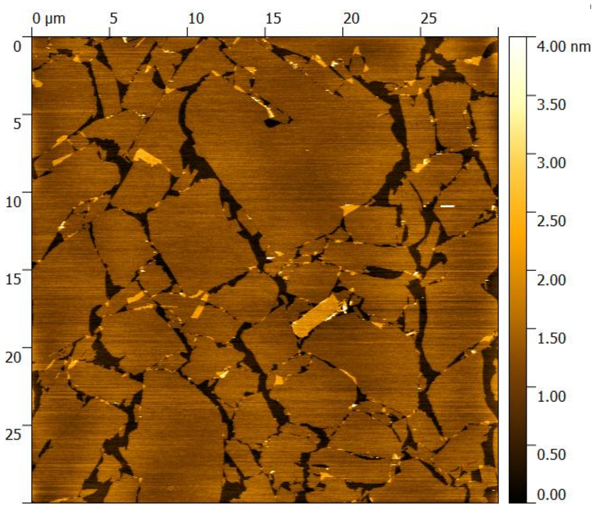

2 minutes

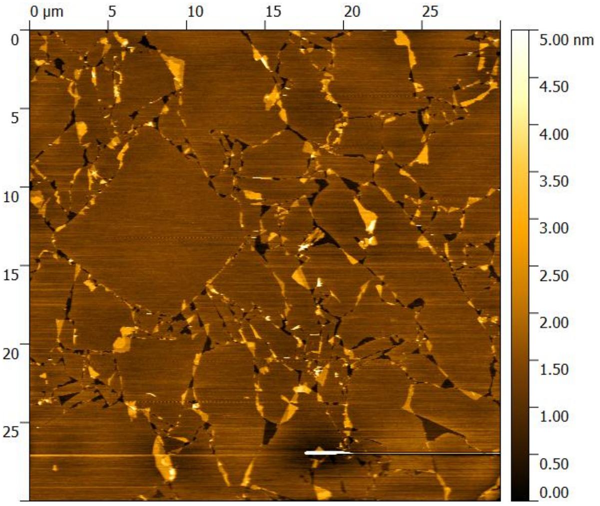

5 minutes

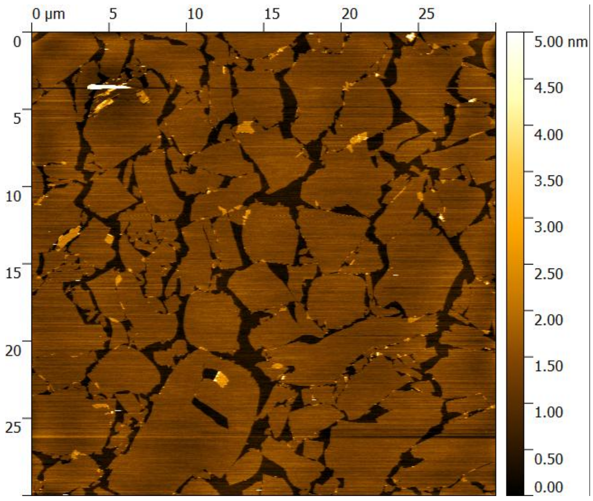

10 minutes

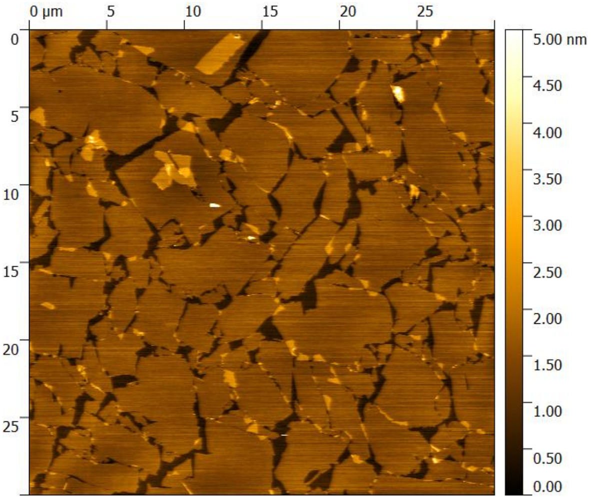

20 minutes

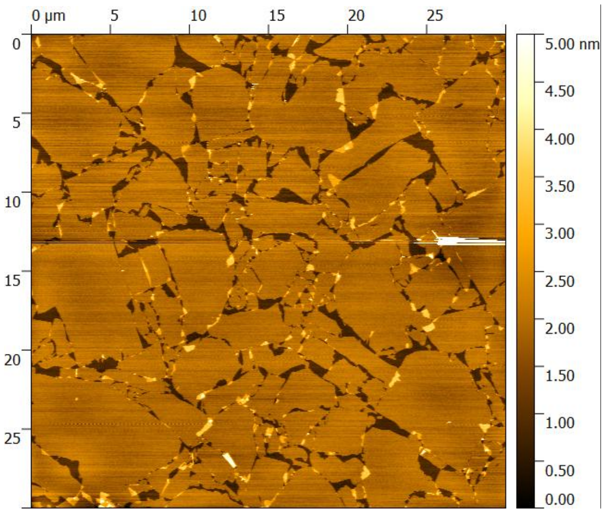

30 minutes

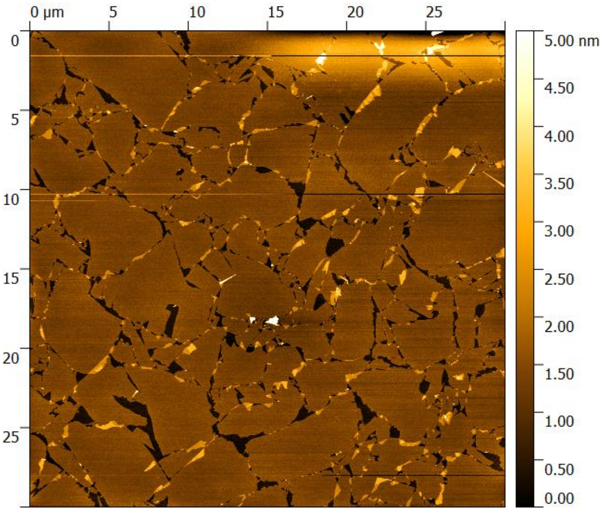

1 hour

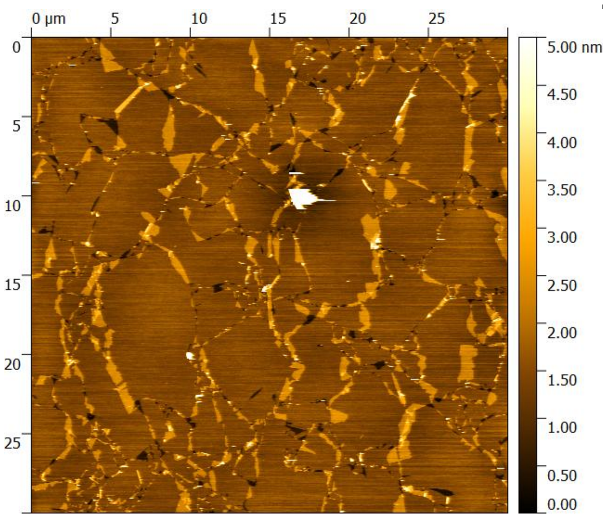

2 hours

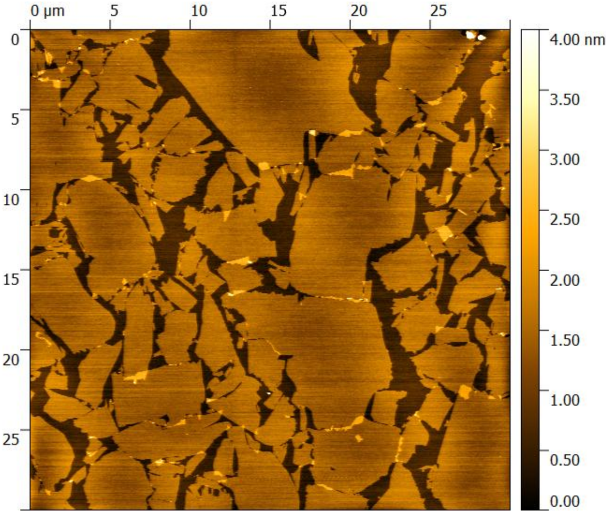

3 hours

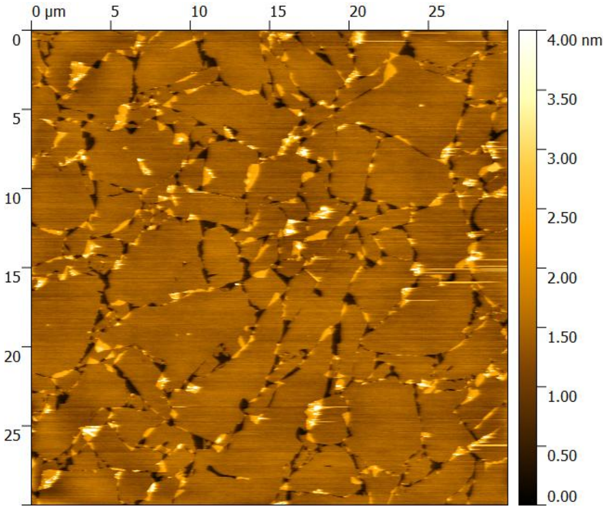

6 hours

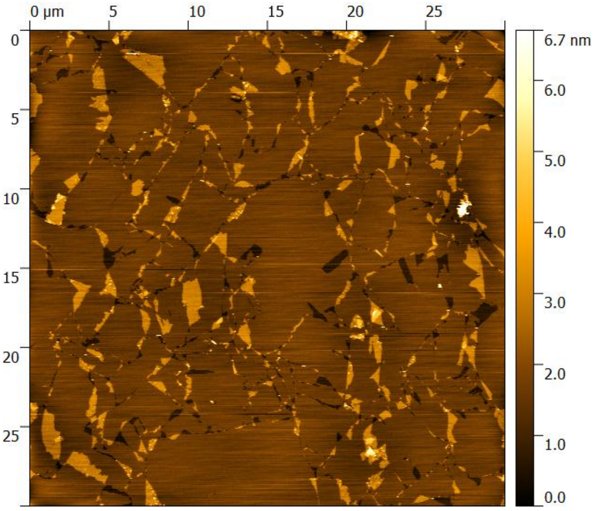

1 day

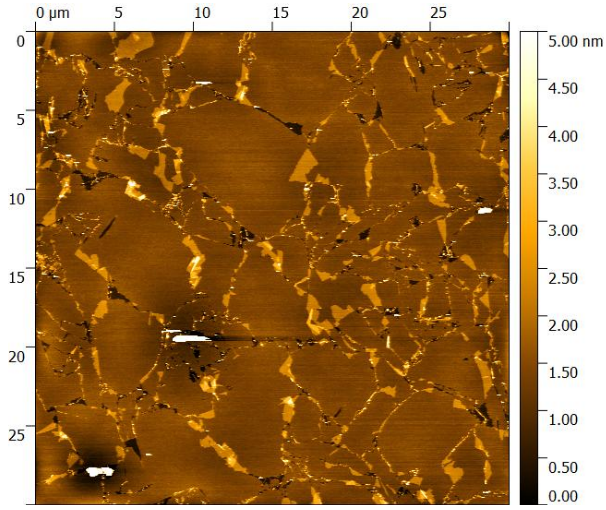

1 week

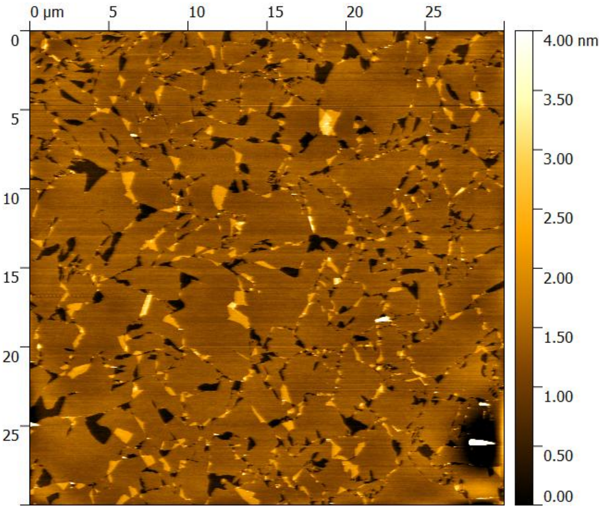

2 weeks